bioRxiv preprint doi: https://doi.org/10.1101/2022.02.17.480766; this version posted February 20, 2022. The copyright holder for this preprint (which was not certified by peer review) is the author/funder, who has granted bioRxiv a license to display the preprint in perpetuity. It is made available under aCC-BY 4.0 International license.

Title: Neuromodulation due to propofol affects anesthetic oscillatory coupling

Authors: Austin E. Soplata[1,2,3], Michelle M. McCarthy[2], Elie M. Adam[2], Patrick L. Purdon[3], Emery N. Brown[3,4,5], Nancy Kopell[2]

Affiliations:

1. Graduate Program for Neuroscience, Boston University, Boston, MA, USA

2. Department of Mathematics & Statistics, Boston University, Boston, MA, USA

3. Department of Anesthesia, Critical Care and Pain Medicine, Massachusetts General Hospital, Harvard Medical School, Boston, MA, USA

4. Department of Brain and Cognitive Sciences, Massachusetts Institute of Technology, Cambridge, MA, USA

5. Institute for Medical Engineering and Science, Massachusetts Institute of Technology, Cambridge, MA, USA

Contributions:

Austin E. Soplata: Conceptualization, Data curation, Investigation, Methodology, Software, Analysis, Validation, Visualization, Writing, Editing. Michelle M. McCarthy: Conceptualization, Analysis, Writing, Editing. Elie M. Adam: Software, Visualization, Analysis, Editing. Patrick . Purdon: Funding acquisition, Data curation, Project administration, Supervision, Editing. Emery N. Brown: Funding acquisition, Project administration, Supervision, Editing. Nancy Kopell: Conceptualization, Analysis, Funding acquisition, Project administration, Supervision, Writing, Editing.

Running Head: Neuromodulation due to propofol affects anes. osc. coupling

Key Words: anesthesia, thalamocortical oscillations, oscillatory coupling, propofol, thalamus

bioRxiv preprint doi: https://doi.org/10.1101/2022.02.17.480766; this version posted February 20, 2022. The copyright holder for this preprint (which was not certified by peer review) is the author/funder, who has granted bioRxiv a license to display the preprint in perpetuity. It is made available under aCC-BY 4.0 International license.

Abstract

The anesthetic propofol produces prominent oscillatory signatures on the EEG. Despite the strong correlation between oscillations and the anesthetic state, the fundamental mechanisms of this unconsciousness remain unknown. On the EEG, propofol elicits alpha oscillations (8-14 Hz), slow oscillations (0.5-2.0 Hz), and dose-dependent phase-amplitude coupling (PAC) between these rhythms. A low enough dose causes "trough-max" PAC, where alpha oscillation amplitude is consistently maximal during slow troughs; this occurs at the same time as arousable unconsciousness. A high enough dose causes consistent "peak-max" PAC, where alpha amplitude is maximal during the slow peak, at the same time as unarousable unconsciousness. Much of the anesthetic state is dominated by a mixture of both states. Using thalamocortical Hodgkin-Huxley simulations, we show that, in addition to propofol effects on $GABA_A$ synapses and thalamocortical H-currents, propofol-induced changes to neuromodulation may generate LFP oscillations and their dose-dependent coupling. We show this for acetylcholine specifically, though other neuromodulators may produce the same effects. We find that LFP- and EEG-relevant synapses of local thalamocortical circuits stochastically display either trough-max or peak-max PAC on any given slow cycle. Trough-max PAC signals are present only in thalamocortical synaptic currents, and not identifiable via membrane potentials alone. PAC preference depends critically on the neuromodulatory state, which is dose-dependent: high doses are associated with statistically more peak-max than trough-max, and vice-versa. This is caused by increased cortical synchronization at higher doses. Our results have important consequences for analyzing LFP/EEG data, in that local network trough- or peak-max may only be seen on a cycle-by-cycle basis, and not when averaging. We hypothesize that this increased cortical

bioRxiv preprint doi: https://doi.org/10.1101/2022.02.17.480766; this version posted February 20, 2022. The copyright holder for this preprint (which was not certified by peer review) is the author/funder, who has granted bioRxiv a license to display the preprint in perpetuity. It is made available under aCC-BY 4.0 International license.

synchronization leads to an inability to process signals in a flexible manner needed for awake cognition.

New & Noteworthy

We simulate biophysical neural networks to investigate how the anesthetic propofol enables alpha and slow oscillations to emerge and interact. Direct effects of propofol on inhibition and indirect effects on acetylcholine level are necessary for dose-dependent emergence and coupling of these rhythms. Local groups of anesthetized cells behave with more complexity than global EEG would suggest. Higher doses are associated with more cortical synchrony, which may underlie the reduced ability to respond to stimuli.

Introduction

Reversible loss of consciousness is the primary aim of all anesthetic agents. Loss of consciousness with the anesthetic propofol is dose-dependent, with lower doses of propofol leading to limited, “arousable” unconsciousness (Purdon et al. 2013; Mukamel et al. 2014; Stephen et al. 2020; Gaskell et al. 2017). For example, with lower doses of propofol, subjects may display decreased arousal but retain their ability to respond to auditory cues if a painful stimulus is applied (Gaskell et al. 2017), or slowly lose their ability to respond (Purdon et al. 2013; Mukamel et al. 2014). In contrast, high-dose propofol administration anesthetizes patients into deep, “unarousable” unconsciousness (Purdon et al. 2013; Mukamel et al. 2014; Gaskell et al. 2017; Stephen et al. 2020).

bioRxiv preprint doi: https://doi.org/10.1101/2022.02.17.480766; this version posted February 20, 2022. The copyright holder for this preprint (which was not certified by peer review) is the author/funder, who has granted bioRxiv a license to display the preprint in perpetuity. It is made available under aCC-BY 4.0 International license.

The EEG during propofol anesthesia is dominated by slow (0.5-2.0 Hz) and alpha (8-14 Hz) oscillations (Purdon et al. 2013; Mukamel et al. 2014). Studies suggest that phase-amplitude coupling (PAC) between slow and alpha oscillations may be an indicator of depth of anesthesia (Purdon et al. 2013; Mukamel et al. 2014). At a sufficiently low dose of propofol, alpha amplitude is maximal during the trough of the slow phase, creating “trough-max” PAC. In contrast, at sufficiently high doses of propofol, alpha amplitude is maximal during the peak of the slow phase, creating “peak-max” PAC (Mukamel et al. 2014). However, large periods of time under propofol do not correspond to either of those states on the temporal scale of spectrogram analysis, instead displaying indeterminant PAC.

In this computational modeling paper, we show that the notions of alpha-slow trough-max and peak-max PAC exist on the fine timescale of single slow periods locally in space. In local networks, each slow period can exhibit either trough- or peak-max randomly changing in time during the same simulation. We also show that the statistics of these changes are dose-dependent, with higher doses of propofol corresponding to a larger percentage of peak-max rather than trough-max cycles. An important finding of the work is that the statistics of the two PAC states were strongly influenced by the synchrony of the cortical cells. Thus, the depth of anesthesia, measured over a long timescale, corresponds to the statistics of trough- and peak-max states, not a global switch between one state and the other.

We base our model on previous models suggesting thalamocortical involvement in the production of propofol slow and alpha oscillations and their coupling (Soplata et al. 2017). Our previous model treated the cortical dynamics strictly as inputs to the thalamic dynamics. Here,

bioRxiv preprint doi: https://doi.org/10.1101/2022.02.17.480766; this version posted February 20, 2022. The copyright holder for this preprint (which was not certified by peer review) is the author/funder, who has granted bioRxiv a license to display the preprint in perpetuity. It is made available under aCC-BY 4.0 International license.

we use a full thalamocortical model with feedforward and feedback connections, and the results depend on these connections. Our thalamic model is derived from (Soplata et al. 2017) and our slow-oscillation-producing cortical model is built on (Compte et al. 2003) (for justification of this cortical slow model, see Methods). The thalamus-to-cortex connections play a prominent role in the synchronization of cortical spiking, which promotes the transition to peak-max.

Our model includes both direct and indirect effects of propofol: The direct effects are those that affect $GABA_A$ inhibition and thalamocortical cell (TC) H-current, while the indirect effects are from its effects on neuromodulation. We focus on acetylcholine (ACh), which propofol is known to decrease (Kikuchi et al. 1998; Meuret et al. 2000; Nemoto et al. 2013; Pal and Mashour 2021; Luo et al. 2020). In the model, ACh affects several currents, but we find that the essential change is the increase in thalamocortical synaptic strength. ACh-mediated increases in thalamocortical synaptic strength lead to greater cortical synchrony and a statistical shift in the proportion of cycles in trough-max versus peak-max. Other neuromodulators may also be involved, especially those that affect thalamocortical strength.

Results

Modeling Objectives and Model Description

The aim of our modeling is to explain the dynamic mechanisms underlying the changing PAC seen in experimental data during a large proportion of the anesthetic state under propofol, as illustrated in Figure 1 from approximately time 0 to 45 minutes. Prominent alpha and slow

bioRxiv preprint doi: https://doi.org/10.1101/2022.02.17.480766; this version posted February 20, 2022. The copyright holder for this preprint (which was not certified by peer review) is the author/funder, who has granted bioRxiv a license to display the preprint in perpetuity. It is made available under aCC-BY 4.0 International license.

oscillations appear in the EEG of patients under propofol, as shown in Figure 1 A and B. The PAC between alpha and slow changes over time as the dose is increased. Except for very high doses, the PAC is neither wholly trough-max nor wholly peak-max, as shown in Figure 1 B and D. As we will show, our model reproduces alpha and slow frequencies as well as the mix of trough-max and peak-max.

Our network is composed of 20 Hodgkin-Huxley-type thalamocortical cells (TC), 20 thalamic reticular neurons (TRN), 100 cortical pyramidal soma cell compartments (PYso), 100 cortical pyramidal dendritic cell compartments (PYdr), and 20 cortical interneurons (IN), as illustrated in Figure 2 A (see Methods). We model the effects of propofol by "direct" and "indirect" effects. The direct effects are: increasing $GABA_A$ maximal conductance ($\bar{g}_{GABA_A}$) and $GABA_A$ decay time constant (τ_{GABA_A}) and decreasing TC cell H-current maximal conductance ($\bar{g}_H$) (see Methods) (Soplata et al. 2017). In addition, we model some indirect effects of propofol on neuromodulation, in particular cholinergic modulation, which is known to decrease in the presence of propofol (see Methods and next section) (Kikuchi et al. 1998; Nemoto et al. 2013; Meuret et al. 2000; Pal and Mashour 2021; Luo et al. 2020). The indirect effects are increased intracortical AMPAergic synaptic conductances ($\bar{g}_{AMPA:PY\rightarrow PY}$), TC-to-PY thalamocortical AMPAergic synaptic conductances ($\bar{g}_{AMPA:TC\rightarrow PY}$), and K(Na)-current maximal conductance ($\bar{g}_{K(Na)}$) (see Methods for detail). As we will see, the most important cholinergic effect is the increase in strength of the thalamocortical connections; we hypothesize that other modulators that produce this effect could also produce the same results as in our model. The number of cells in the model is relatively small and is intended to model local activity similar to an LFP signal.

bioRxiv preprint doi: https://doi.org/10.1101/2022.02.17.480766; this version posted February 20, 2022. The copyright holder for this preprint (which was not certified by peer review) is the author/funder, who has granted bioRxiv a license to display the preprint in perpetuity. It is made available under aCC-BY 4.0 International license.

The LFP of the model is produced by two sets of synapses: thalamocortical (TC→PY) and intracortical (PY→PY), both targeting the dendrites of cortical pyramidal cells (see Methods).

The parameters were chosen such that in a baseline condition without propofol, the model produces a depolarized relay-mode state under weak, constant applied current, as shown in Figure 2 B. This simulation exhibits non-bursting, tonic spiking in both the cortex and thalamus as spikes are relayed between regions. Neither region shows high-activity bursts or long periods of quiescence as one would expect in sleep or anesthetized states. This baseline simulation does not exhibit either slow or alpha oscillations spiking.

Direct effects do not produce alpha and slow oscillations

Our previous work (Soplata et al. 2017) showed that the "direct" effects of propofol were sufficient for enabling alpha oscillations in a thalamic model with an artificial cortical input. In contrast, our current model expresses neither UP/DOWN slow states nor alpha oscillations in response to the direct effects of propofol across many different values of $GABA_A$ and $\bar{g}_H$ parameter values, as shown in

Figure 3 A. The lack of DOWN states allows the cortex to continue to send strong, consistent excitation to the anesthetized thalamus, thus interfering with thalamic bursting and propofol alpha oscillations, as shown in

Figure 3 B and C. More details about this mechanism are in Ancillary Information 1.

bioRxiv preprint doi: https://doi.org/10.1101/2022.02.17.480766; this version posted February 20, 2022. The copyright holder for this preprint (which was not certified by peer review) is the author/funder, who has granted bioRxiv a license to display the preprint in perpetuity. It is made available under aCC-BY 4.0 International license.

Neuromodulatory effects enable both alpha and slow oscillations

Since direct propofol effects are not able to produce propofol oscillations in our model of the depolarized relay state, we expand our propofol modeling to also include its "indirect" effects. Our indirect effects are modeled as a decrease of cortical ACh in three ways: increasing PY cell K(Na)-current maximal conductance ($\bar{g}_{K(Na)}$) (Compte et al. 2003; Benita et al. 2012), increasing intracortical PY→PY AMPAergic synaptic maximal conductance ($\bar{g}_{AMPA:PY\rightarrow PY}$) (Krishnan et al. 2016), and increasing thalamocortical TC→PY AMPAergic synaptic maximal conductance ($\bar{g}_{AMPA:TC\rightarrow PY}$), the latter by way of muscarinic ACh receptors (Kruglikov and Rudy 2008; Favero, Varghese, and Castro-Alamancos 2012).

With the addition of the indirect effects, the model is able to generate propofol slow and alpha oscillations observed in both the model LFP and the spiking in Figure 4 A and B. The slow oscillation of our cortical model relies on $\bar{g}_{K(Na)}$, as in the sleep slow model from which it was derived (Compte et al. 2003). Random excitation triggers a cortical UP state, during which intracellular sodium builds up, activating the K(Na)-current. This current then terminates the UP state and transitions the pyramidal cells to silent, hyperpolarized DOWN states, just as in the original work (Compte et al. 2003). We assume in our model that these cortical UP and DOWN states correspond, respectively, to the peak and trough of EEG / LFP slow as in natural sleep slow oscillations (Vincenzo Crunelli and Hughes 2010; Cash et al. 2009; Amzica and Steriade 2002).

bioRxiv preprint doi: https://doi.org/10.1101/2022.02.17.480766; this version posted February 20, 2022. The copyright holder for this preprint (which was not certified by peer review) is the author/funder, who has granted bioRxiv a license to display the preprint in perpetuity. It is made available under aCC-BY 4.0 International license.

In addition to slow oscillations, propofol-induced neuromodulation enables thalamic alpha oscillations, as shown in Figure 4. In each slow cycle, the alpha spiking appears in one of two patterns depending on individual slow cycles. During some individual slow cycles, thalamic alpha is present during the cortical DOWN state (blue highlights in Figure 4), while during other slow cycles, thalamic alpha is absent from the cortical DOWN state (orange highlights in Figure 4). We refer to the former as trough-max and the latter as peak-max: the two switch apparently randomly on the timescale of seconds, consistent with Figure 1 B. In peak-max, the thalamic alpha exists only in a small range of phases of the slow oscillation. In trough-max, the alpha is spread out over almost the entire slow oscillation cycle, with the most power where cortex is in the DOWN state, making the duration of the alpha longer than in peak-max periods. Though "peak-max" and "trough-max" are defined here in terms of spiking patterns, we will show below that the LFP matches this nomenclature: high alpha in spiking is at the peak of the LFP during peak-max, and high alpha in spiking is around the trough of the LFP during trough-max.

In the next sections, we will characterize how peak-max and trough-max time periods come about, locally in time in both the spiking and the LFP. For this analysis, we need to understand how the LFP is produced during each of the states by looking at the two kinds of synaptic currents in the model that constitute the LFP: thalamocortical and intracortical synapses that target the pyramidal cell dendrites.

Phase-amplitude coupling between alpha and slow oscillations during peak-max

bioRxiv preprint doi: https://doi.org/10.1101/2022.02.17.480766; this version posted February 20, 2022. The copyright holder for this preprint (which was not certified by peer review) is the author/funder, who has granted bioRxiv a license to display the preprint in perpetuity. It is made available under aCC-BY 4.0 International license.

During peak-max, thalamic alpha oscillations occur in the spiking only near or during cortical UP states, as shown in Figure 5. Immediately before a cortical UP state, thalamic cells spontaneously burst at the propofol alpha frequency, as shown Figure 5 C. These thalamic bursts initiate a cortical UP state in which the firing is relatively synchronous. The resulting PY→TC depolarization from the synchronous cortical UP is strong enough to depolarize the TC cells into their silent, depolarized state, also known as the "thalamic relay-mode" (see section below "Cortical synchronization modulates thalamic state and is modulated by thalamocortical feedback"). This terminates the thalamic alpha bursting, causing the TC cells to cease oscillating. Loss of TC activity contributes to cessation of cortical spiking and the emergence of the DOWN state. Once both cortical and thalamic cells are quiescent for long enough, the TC cells spontaneously hyperpolarize and initiate bursts again, resetting the cycle.

We now consider the synaptic currents onto the pyramidal cell dendrites, the constituents currents of the LFP model, during peak-max as shown in Figure 6. During peak-max, both TC→PY and PY→PY synaptic currents are maximal during the cortical UP states, as shown in Figure 4 B and Figure 6. Since thalamic alpha is generated only around the cortical UP, at the peak of the LFP, the coupling between alpha and slow is strong during peak-max, as shown in Figure 4 B, Figure 6 D and Ancillary Information 1. Thus, during peak-max, there is a cooperation in the coupling signal.

To quantify the amount and preferred slow-phase of alpha power in our LFP signal during this time period, we used the Modulation Index (MI) method (Tort et al. 2010; Purdon et al. 2013) as shown in Figure 7 D. Across the different slow cycles of the combined TC→PY and PY→PY

bioRxiv preprint doi: https://doi.org/10.1101/2022.02.17.480766; this version posted February 20, 2022. The copyright holder for this preprint (which was not certified by peer review) is the author/funder, who has granted bioRxiv a license to display the preprint in perpetuity. It is made available under aCC-BY 4.0 International license.

synaptic current comodulogram, the alpha magnitude of the combined synaptic current switches its preference between 0 (middle) on the slow phase, corresponding to the slow peak, and ±π (edges), corresponding to the slow trough. During the indicated time period, which corresponds to the orange peak-max time period in 6 A, this current tends towards the slow peak phase instead of the slow trough phase, illustrated by the coupling skewing towards the center. Our simulated peak-max signature highlighted in Figure 7 D is similar to peak-max times in Figure 1 of this work.

Phase-amplitude coupling between alpha and slow oscillations during trough-max

We next examine how the alpha and slow interact during the blue trough-max time periods. During this time, cortical spiking is not tightly synchronized, as shown in Figure 5 A and D. Due to this less synchronized cortical excitation, the thalamus is able to remain hyperpolarized enough during trough-max to have uninterrupted alpha bursting.

During this trough-max time period, target PYdr compartments exhibit slow oscillations, as shown in Figure 8 B, while the cortically projecting TC cells exhibit alpha oscillations during the cortical DOWN state, as shown in Figure 8 C. The resulting TC→PY synaptic current is shown in Figure 8 D. The amplitude of the total TC→PY synaptic current fluctuates both with alpha bursts from the thalamus and on a slow timescale due to the fluctuation of the membrane voltage of the PY cells. During cortical slow fluctuations, the synaptic current is maximal during the DOWN/non-spiking (trough) phase of the target cortical cell, as indicated by dashed lines in Figure 8 D and E. This is likely due to the less-synchronous cortex allowing for thalamic alpha to

bioRxiv preprint doi: https://doi.org/10.1101/2022.02.17.480766; this version posted February 20, 2022. The copyright holder for this preprint (which was not certified by peer review) is the author/funder, who has granted bioRxiv a license to display the preprint in perpetuity. It is made available under aCC-BY 4.0 International license.

occur for more of the phase than in peak-max. We note that neither the spiking of the TC nor PY cells alone display alpha-slow coupling; the coupling is evident only in the synaptic interaction between the TC cells and the pyramidal cell dendrites.

In contrast to peak-max, synaptic intracortical currents have very different behavior than synaptic thalamocortical currents during trough-max, as shown in Figure 8 and Figure 9. During peak-max, intracortical currents are maximal during the slow peak or UP state (Figure 8 F-H), whereas thalamocortical currents are maximal during the slow trough or DOWN state (Figure 8 B-E). Despite these synaptic currents competing with each other (Figure 9 A and B), the thalamocortical current is an order of magnitude stronger than the intracortical current (Figure 9 C), causing the combination of these currents to exhibit trough-max (Figure 9 D).

Cortical synchronization modulates thalamic state and is modulated by thalamocortical feedback

There are two obvious dynamic differences between trough-max and peak-max: the latter displays more cortical synchronization and the thalamus undergoes periods of silence similar to cortical DOWN states, as shown in Figure 5 and Figure 10. These two phenomena are causally related: during peak-max, the cortical cells are highly synchronized, giving more excitation to the thalamus during the cortical UP state, which depolarizes the thalamus out of its alpha bursting mode into silent depolarization, producing a DOWN state in thalamus. In the absence of cortical synchrony, the thalamus remains more hyperpolarized, producing continuous alpha during cortical DOWN states. Furthermore, in peak-max, the existence of the thalamic DOWN state implies that the cortex receives less excitation during that period, causing the cortex to fire

bioRxiv preprint doi: https://doi.org/10.1101/2022.02.17.480766; this version posted February 20, 2022. The copyright holder for this preprint (which was not certified by peer review) is the author/funder, who has granted bioRxiv a license to display the preprint in perpetuity. It is made available under aCC-BY 4.0 International license.

more synchronously during the next UP, since PY cells have not been made to prematurely fire. Thus, there is a reciprocal relationship between spiking synchrony in the cortex and the decrease of alpha in the thalamus.

The level of cortical synchrony of a slow cycle is produced not only by thalamocortical feedback but also by a stochastic process determined by many factors. These other factors allow switches between peak-max and trough-max on a slow cycle-by-cycle basis. In particular, there is a seemingly chaotic response to similar but different initial conditions: different simulations express very different proportions of time spent in trough-max or peak-max (low or high synchrony). We hypothesize that variables associated with activity of pyramidal cells in the peak-max cortical DOWN state, in which a few pyramidal cells always remain spiking, contribute to the switch from peak-max to trough-max. However, obtaining a complete understanding of the slow cycle-to-cycle variations is outside the scope of this work.

Neuromodulation can change preferred PAC regime via changing thalamocortical feedback

By modeling higher dose propofol via increasing the indirect effects of ACh, we find that the network shifted from preferring trough-max to peak-max, as shown in Figure 11. To show this, we ran 200 simulations with the previous parameters and random initial conditions, and 200 more simulations with the same parameters, except for increases in $\bar{g}_{\mathrm{AMPA:TC\rightarrow PY}}$, $\bar{g}_{\mathrm{AMPA:PY\rightarrow PY}}$, and $\bar{g}_{\mathrm{K(Na)}}$, which model further increases in propofol via a decrease in cholinergic modulation. We then averaged the amount of time each simulation exhibited trough-max (data in

bioRxiv preprint doi: https://doi.org/10.1101/2022.02.17.480766; this version posted February 20, 2022. The copyright holder for this preprint (which was not certified by peer review) is the author/funder, who has granted bioRxiv a license to display the preprint in perpetuity. It is made available under aCC-BY 4.0 International license.

Supplementary Data 1), since any time not spent in trough-max exhibited peak-max. The lower dose propofol simulations show a slight preference for trough-max over peak-max, with 53% of the time spent in trough-max. In high-dose simulations, the system shifts to a clear preference for peak-max, with trough-max occurring only 27% of the time. There is a high degree of variability among individual simulations, with the proportion of time spent in trough-max having a standard deviation of 20% in the low-dose case and 13% in the high-dose case.

To understand the cause of this PAC preference shift, we examined each of the propofol indirect effects individually. Starting with low-dose parameters, we changed one indirect effect parameter at a time (i.e., $\bar{g}_{\mathrm{AMPA:TC\rightarrow PY}}$, $\bar{g}_{\mathrm{AMPA:PY\rightarrow PY}}$, or $\bar{g}_{\mathrm{K(Na)}}$) and ran 200 more simulations each. With a high dose level of $\bar{g}_{\mathrm{AMPA:TC\rightarrow PY}}$, the proportion of time spent in trough-max decreases to 30% (± 13%), similar to the decrease from low-dose to high-dose propofol with all indirect effects increased. In contrast, with a high-dose level of $\bar{g}_{\mathrm{AMPA:PY\rightarrow PY}}$ or $\bar{g}_{\mathrm{K(Na)}}$, the proportion of time spent in trough-max is 50% (± 19%) or 54% (± 18%), respectively. This strongly suggests that changes to thalamocortical synaptic strength are the primary cause of the change in preferred PAC in our model (parameters in Methods and Appendix, data in Supplemental Data 1).

The shift to peak-max when $\bar{g}_{\mathrm{AMPA:TC\rightarrow PY}}$ increases is likely due to the increased ability of thalamic bursting to recruit more cortical cells into the synchronized cortical UP state. These synchronized cortical cells send more feedback excitation to TC cells, causing them to enter their depolarized silent state and begin the mutually-enforcing patterns of thalamocortical and corticothalamic interactions that characterize peak max.

bioRxiv preprint doi: https://doi.org/10.1101/2022.02.17.480766; this version posted February 20, 2022. The copyright holder for this preprint (which was not certified by peer review) is the author/funder, who has granted bioRxiv a license to display the preprint in perpetuity. It is made available under aCC-BY 4.0 International license.

Discussion

Overview

In this work, we simulate a thalamocortical network of Hodgkin-Huxley cells to understand the propofol anesthetic state during which neither trough-max nor peak-max appears to dominate the EEG, though the statistics of these two states change with dose. We find that both the direct effects of propofol on cellular membrane and inhibitory dynamics as well as the indirect effects of propofol mediated by ACh are necessary for producing slow oscillations, alpha oscillation, and their coupling. Slow oscillations generated by cortex and alpha oscillations generated by thalamus couple during propofol states, but do not form stable, long-lasting PAC regimes at the LFP level. The alpha-slow PAC can change from slow cycle to slow cycle in a manner that appeared to be stochastic, with a slight preference for trough-max with a lower dose and a strong preference for peak-max at a higher dose. We found the PAC type distribution depends on the synchronization of the cortex and, therefore, the cortical signal given to the thalamus. At the higher dose of propofol, the increase in $\bar{g}_{\mathrm{AMPA:TC\rightarrow PY}}$, an indirect effect of propofol due to ACh, is highly influential in changing the preferred PAC type in favor of peak-max. Increasing $\bar{g}_{\mathrm{AMPA:TC\rightarrow PY}}$ leads to higher synchronization of the cortical pyramidal cells, which leads to stronger and more focused feedback to the thalamus.

Prior work and thalamocortical feedback

bioRxiv preprint doi: https://doi.org/10.1101/2022.02.17.480766; this version posted February 20, 2022. The copyright holder for this preprint (which was not certified by peer review) is the author/funder, who has granted bioRxiv a license to display the preprint in perpetuity. It is made available under aCC-BY 4.0 International license.

While prior modeling demonstrated thalamocortical circuits could produce propofol alpha oscillations (Ching et al. 2010; Vijayan et al. 2013), or propofol alpha and slow (Krishnan et al. 2016), our previous work (Soplata et al. 2017) was the first modeling investigation into the unique alpha-slow PAC dynamics of propofol of which we are aware. Our current thalamocortical model includes feedback from thalamus to cortex, leading to updates of several predictions pertaining to propofol alpha-slow PAC as well as to new mechanistic insights into the role of thalamocortical feedback in network dynamics related to loss of consciousness.

Our prior model predicted propofol-alpha generation in thalamus due to the direct effects of propofol. Our current thalamocortical model supports thalamic generation of alpha but additionally requires the indirect effect of propofol lowering ACh and decreasing cortical firing to generate this alpha. In the prior thalamus-only model, thalamic alpha emerged only during the DOWN state in trough-max and only during the UP state in peak-max. In the current model, in which the hyperpolarization level of the thalamus is partially controlled by the cortex, we find that, during trough-max, the thalamus does not hyperpolarize enough to stop spiking during the UP state; rather, the thalamus continues to burst in alpha in both cortical UP and DOWN states. We also find that, during peak-max, the thalamic silence during the DOWN state is due to depolarization from corticothalamic excitation, rather than hyperpolarization as suggested by the thalamus-only model. The natural switching between trough-max and peak-max found in the current model relies on thalamocortical feedback, in the shape of partial control of cortical dynamics by the thalamus not available in the prior model.

Additionally, cortical synchronization, which requires thalamocortical feedback, plays a key role

bioRxiv preprint doi: https://doi.org/10.1101/2022.02.17.480766; this version posted February 20, 2022. The copyright holder for this preprint (which was not certified by peer review) is the author/funder, who has granted bioRxiv a license to display the preprint in perpetuity. It is made available under aCC-BY 4.0 International license.

in determining the PAC regime. However, ultimately the PAC regime expressed in each slow cycle is a product of many factors including randomness, and it is outside the scope of this work to evaluate all the determinants of peak-max versus trough-max LFP PAC. Many synaptic and intrinsic factors across different regions could have strong effects on the network dynamics. Even small perturbations to the initial conditions result in radically different simulations, indicating chaotic outcomes in the time course of our simulated LFP PAC. This is similar to the slow oscillations in natural sleep, in that different components of the sleep slow oscillation arise out of different, possibly complementary mechanisms rather than any single set (Neske 2016).

Detectability of cycle-by-cycle PAC

In Figure 1 it is surprising that we see cycle by cycle changes in EEG experiments. The EEG may be considered to be an average of many LFP signals (Nunez and Srinivasan 2006); therefore, one might expect that cycle-by-cycle LFP PAC changes could be washed out by the EEG spatial averaging. The fact that we do see cycle-by-cycle changes suggests that there may be significant synchrony locally around each EEG electrode.

If we are correct that TC→PY synapses are the main contributor to the LFP during trough-max, this PAC may not be observable from individual, cortical, or thalamic cell voltages or spike recordings alone. Instead, the EEG signature of trough-max may arise exclusively from TC→PY-generated synaptic current dipoles within the dendrites of pyramidal cells. Therefore, trough-max may appear in cortical electric field measures or spike-field coherence between

bioRxiv preprint doi: https://doi.org/10.1101/2022.02.17.480766; this version posted February 20, 2022. The copyright holder for this preprint (which was not certified by peer review) is the author/funder, who has granted bioRxiv a license to display the preprint in perpetuity. It is made available under aCC-BY 4.0 International license.

thalamic spikes and cortical fields, but possibly not spike-field coherence between cortical spikes and cortical fields.

Spatiotemporal heterogeneity and future modeling

Heterogeneity in TC→PY and PY→PY strength and connectivity across cortical regions and layers may contribute to diversity in cortical synchronization levels (Redinbaugh et al. 2020; Malekmohammadi et al. 2019) and therefore diversity in local PAC. Our simulations indicate that different doses of propofol tend to express different PAC regimes on a small spatial scale. Our results also suggest that under propofol, different local cortical networks may, on a fast timescale, switch between trough-max or peak-max at the LFP level in the cortex even while a regional EEG signal predominantly shows a single type of dose-dependent PAC. Our model suggests that during high-dose propofol when the comodulogram predominantly expresses EEG peak-max, the EEG can still exhibit some trough-max PAC cycles, as we see in Figure 1 B.

By introducing region-specific heterogeneity to cortex (e.g., sensory and higher-order) and thalamus (e.g., core and matrix), future simulations may be able to investigate the significant spatiotemporal changes between low- and high-dose propofol. “Anteriorization” is a well-known phenomenon where propofol administration initially leads to the loss of awake, occipital alpha and an increase in frontal alpha (Tinker, Sharbrough, and Michenfelder 1977; Cimenser et al. 2011; Vijayan et al. 2013). This frontal alpha is at its strongest and most persistent state during low-dose EEG trough-max, before spreading to become region-nonspecific during high-dose

bioRxiv preprint doi: https://doi.org/10.1101/2022.02.17.480766; this version posted February 20, 2022. The copyright holder for this preprint (which was not certified by peer review) is the author/funder, who has granted bioRxiv a license to display the preprint in perpetuity. It is made available under aCC-BY 4.0 International license.

EEG peak-max PAC (Cimenser et al. 2011; Purdon et al. 2013; Mukamel et al. 2014; Stephen et al. 2020) and decreasing in power with increasing dose (Gutiérrez et al. 2022). Slow power is also greater during high-dose than low-dose propofol (Purdon et al. 2013; Mukamel et al. 2014; Mhuircheartaigh et al. 2013; Lee et al. 2017) and may modulate higher frequencies more in frontal regions during peak-max (Stephen et al. 2020). Modeling prefrontal cortex specifically will allow us to probe why trough-max is prevalent in frontal cortex (Mukamel et al. 2014), why there is stronger frontal slow modulation during peak-max (Stephen et al. 2020), and why there is increased thalamocortical alpha coherence in this region (Flores et al. 2017). Simultaneously modeling of sensory cortex will allow us to explore coherence, phase (Malekmohammadi et al. 2019), and firing rate (Krom et al. 2020) discrepancies found between frontal and sensory regions under anesthesia. Understanding how heterogeneity affects cross-cortical communication and frontal cortex specifically may help to validate theories of loss of consciousness, including frontoparietal disconnection (Hudetz and Mashour 2016) and similar connectivity changes (Banks et al. 2020), brainstem changes to neuromodulation (Brown, Purdon, and Van Dort 2011), alpha blocking of processing (Palva and Palva 2007), and slow oscillation control of activity (Gemignani et al. 2015; Stephen et al. 2020).

Propofol, slow oscillations, and neuromodulation

A notable interpretation of this model is that the anesthetic effects depend on the indirect neuromodulatory effects of ACh as much as on the direct effects on $GABA_A$ inhibition and the TC cell H-currents; however, any other modulator that increases the strength of coupling from thalamus to cortex will likely have the same effect. While we restrict our investigation here to

bioRxiv preprint doi: https://doi.org/10.1101/2022.02.17.480766; this version posted February 20, 2022. The copyright holder for this preprint (which was not certified by peer review) is the author/funder, who has granted bioRxiv a license to display the preprint in perpetuity. It is made available under aCC-BY 4.0 International license.

propofol cholinergic changes, propofol likely also utilizes known slow mechanisms via its effects on non-cholinergic brainstem neuromodulatory systems. Propofol affects not just the cholinergic sources in the basal forebrain, laterodorsal tegmental area, and pedunculopontine tegmental area, but, through enhancing inhibition by the pre-optic area, also inhibits the tuberomammillary nucleus, locus coeruleus, dorsal raphe nucleus, ventral periaqueductal gray, and lateral hypothalamus (Brown, Lydic, and Schiff 2010; Brown, Purdon, and Van Dort 2011). These areas respectively provide histamine, norepinephrine, serotonin, dopamine, and orexin/hypocretin to the cortex (Brown, Lydic, and Schiff 2010; Brown, Purdon, and Van Dort 2011). Many of these neuromodulators affect various potassium currents that are critical in known slow models, including the K(Na)-current, the NaP-current, and potassium leak currents (Schwindt, Spain, and Crill 1989; McCormick 1992). These neuromodulators can also affect both excitatory and inhibitory currents in the cortex, and can change the relative impact of thalamocortical synapses (McCormick 1992; Favero, Varghese, and Castro-Alamancos 2012; Kuo and Dringenberg 2008). However, there is still much we do not understand about how these neuromodulators work in concert together (Krishnan et al. 2016). Global $GABA_A$ conductance strength, which is very important in the mechanisms of propofol, has also been found to vary across natural sleep and has been analyzed alongside other neuromodulators in a similar thalamocortical model (Krishnan et al. 2016). Additionally, increasing K(Na) strength decreases the frequency of slow oscillations in this cortical model (Benita et al. 2012), and this current behaves similarly to ATP-dependent K-currents previously used in burst suppression modeling (Cunningham et al. 2006, 200; Ching et al. 2012). Therefore, by further exploring the slow oscillation mechanism in this work and including slow mechanisms impacted by non-cholinergic

bioRxiv preprint doi: https://doi.org/10.1101/2022.02.17.480766; this version posted February 20, 2022. The copyright holder for this preprint (which was not certified by peer review) is the author/funder, who has granted bioRxiv a license to display the preprint in perpetuity. It is made available under aCC-BY 4.0 International license.

and metabolic neuromodulators, it may be possible to augment this model to simulate not just propofol PAC regimes, but also burst suppression.

It is known that the cholinesterase inhibitor physostigmine reverses propofol LOC (Meuret et al. 2000); assuming LOC depends on slow oscillations, our model suggests that the indirect engagement of the K(Na) current by propofol may explain this experimental result. Physostigmine acts to increase ACh levels, which would decrease $\bar{g}_{K(Na)}$ in our model and stop the K(Na)-dependent slow, thus eliminating propofol-induced slow. ACh also acts to weaken thalamocortical connections (Favero, Varghese, and Castro-Alamancos 2012) and therefore release the cortex from over-synchronization; less synchronized states are associated with the awake state. Thus, loss of ACh may be a major contributor to propofol-induced loss of consciousness. The fact that our model requires neuromodulatory changes to produce propofol oscillations and their coupling suggests that the effects of propofol on the brainstem may be critical for its oscillatory phenomena, which is supported by active experimental research on propofol and other anesthetics (Moody et al. 2021; Minert, Yatziv, and Devor 2017; Minert, Baron, and Devor 2020; Muindi et al. 2016; Vlasov et al. 2021). Since the transition from trough-max to peak-max is associated with only lowering ACh in our model, we predict that a smaller dose of physostigmine may promote less peak-max.

In addition to a deeper understanding of the role of ACh in the dynamics of anesthesia, our model makes predictions about effects of localized injections of propofol and ACh receptor antagonist, scopolamine. If propofol is locally injected into the thalamus, and scopolamine is locally injected into the cortex, we predict that propofol slow and alpha oscillations would

bioRxiv preprint doi: https://doi.org/10.1101/2022.02.17.480766; this version posted February 20, 2022. The copyright holder for this preprint (which was not certified by peer review) is the author/funder, who has granted bioRxiv a license to display the preprint in perpetuity. It is made available under aCC-BY 4.0 International license.

appear on the EEG. This would happen due to the cortical decrease in ACh, enabling K(Na)-current activation, thus generating cortical slow, which in combination with the direct effects of propofol in thalamus would enable thalamic alpha. Different doses of scopolamine in this case may be able to induce predominantly EEG trough-max or peak-max as well, depending on how ACh modulation through scopolamine affects thalamocortical synaptic strength.

Propofol, slow oscillations, and sleep

Our work suggests that propofol utilizes not only thalamic spindling mechanisms (Soplata et al. 2017), but also natural sleep slow mechanisms and changes in neuromodulation to produce its oscillatory and PAC effects. The K(Na)-current is the primary mechanism of slow generation in the cortical sleep slow model we used (Sanchez-Vives, Nowak, and McCormick 2000; Schwindt, Spain, and Crill 1989; Compte et al. 2003). Because propofol decreases ACh in the cortex (Kikuchi et al. 1998; Nemoto et al. 2013), and decreasing ACh strengthens the K(Na)-current (Schwindt, Spain, and Crill 1989; McCormick 1992) (see Introduction), indirect cholinergic effects by propofol on this current may contribute to propofol slow generation. Most other slow models rely on a combination of changes to cortical excitatory/inhibitory plasticity and/or the persistent sodium current (NaP) (Bazhenov et al. 2002; Hill and Tononi, Giulio 2004; V. Crunelli et al. 2011; Sanchez-Vives and McCormick 2000; Timofeev et al. 2000; Krishnan et al. 2016). The NaP-current has been shown to be functionally coupled to the K(Na)-current (Hage and Salkoff 2012), and therefore the K(Na)-current may contribute to these mechanisms. Models of slow UP state initiation, also called DOWN-to-UP transitions, rely on random cortical excitation (Timofeev et al. 2000), synaptic plasticity changes (Krishnan et al. 2016; Sanchez-

bioRxiv preprint doi: https://doi.org/10.1101/2022.02.17.480766; this version posted February 20, 2022. The copyright holder for this preprint (which was not certified by peer review) is the author/funder, who has granted bioRxiv a license to display the preprint in perpetuity. It is made available under aCC-BY 4.0 International license.

Vives and McCormick 2000), or TC initiation of cortical slow UP states (V. Crunelli et al. 2011). In our trough-max simulations, persistent thalamic alpha provides constant excitation relative to cortical slow oscillations, enabling UP states to initiate as soon as the hyperpolarizing K(Na)-current in a PY cell has decayed. In our peak-max simulations, however, TC cells exhibit their own silent depolarized states, and upon thalamic re-hyperpolarization, sudden intrinsic thalamic bursting onto a silent cortex enables synchronized cortical UP states. Future work designed to differentiate natural sleep slow versus anesthetic slow mechanisms will enable finer-grained experiments into how the loss of consciousness occurs in these two distinct states.

Propofol, memory consolidation, and aging

Our investigation of these thalamocortical dynamics under propofol may have implications for memory and aging. During natural sleep, memory consolidation onto cortical axo-dendrite connections likely occurs during the nesting of hippocampal ripples during thalamic spindles, which themselves are nested inside thalamocortical sleep slow oscillations (Penagos, Varela, and Wilson 2017). Based on our current and previous work (Soplata et al. 2017), propofol alpha and slow oscillations likely utilize some of the same mechanisms used by these processes. Proper memory consolidation requires correct encoding of worthwhile memories during sleep (Stickgold 2005), but if application of propofol abnormally activates some of the same oscillations in this process, the oscillations of propofol may cause invalid memory consolidation or interfere with synaptic-dendrite networks involved in storing memory. A recent experiment showed promising results in using propofol to disrupt reconsolidation of traumatic memories (Galarza Vallejo et al. 2019), which could help treat Post-Traumatic Stress Disorder patients.

bioRxiv preprint doi: https://doi.org/10.1101/2022.02.17.480766; this version posted February 20, 2022. The copyright holder for this preprint (which was not certified by peer review) is the author/funder, who has granted bioRxiv a license to display the preprint in perpetuity. It is made available under aCC-BY 4.0 International license.

Additionally, alpha power and, to a lesser extent, slow power under propofol may indicate a subject's "brain age" (Purdon et al. 2015). Our modeling predicts that propofol alpha may exclusively arise from the thalamus, and therefore a decrease in propofol alpha power across age could correlate with brain fitness via losses in the ability of the thalamus to burst (Purdon et al. 2015), myelination retention of thalamocortical afferents (Peters 2002), or the strength of thalamocortical synapses onto cortical dendrites (Morrison and Baxter 2012).

Implications for unconsciousness

One unintuitive finding suggested by our model was that TC neurons may be depolarized into "relay mode" during peak-max DOWN states, and could potentially relay sensory information during this window, even during anesthesia. In our simulations, strong corticothalamic excitation after synchronized UP states increased the membrane potential of TC cells during peak-max, as shown in Figure 6. This increase was enough to interrupt the intrinsic alpha bursts of the thalamus, but if this occurs at the same time as strong sensory input spikes, the TC cells may be depolarized enough to briefly relay sensory spiking information up to the cortex. Recently, in humans under low propofol anesthesia, auditory stimuli resulted in wake-like cortical neural activity in primary auditory cortex but not higher-order cortex (Krom et al. 2020). This suggests that some thalamic sensory relay may still occur under propofol anesthesia, even if changes to cross-cortical communication prevent its higher-order processing. Furthermore, in our simulations, peak-max may occur during individual slow cycles of both low- and high-dose propofol, indicating this brief sensory relay may occur at any point during propofol anesthesia (Malekmohammadi et al. 2019; Krom et al. 2020).

bioRxiv preprint doi: https://doi.org/10.1101/2022.02.17.480766; this version posted February 20, 2022. The copyright holder for this preprint (which was not certified by peer review) is the author/funder, who has granted bioRxiv a license to display the preprint in perpetuity. It is made available under aCC-BY 4.0 International license.

Our modeling of how propofol alters coordination of thalamocortical oscillatory activity may help explain how anesthesia leads to arousable and unarousable loss of consciousness. While our model of PAC shows how sensory stimuli can still reach primary regions of cortex (see previous paragraph), it also suggests that there may be large dynamic changes in UP state synchrony among cortical neurons. If thalamic bursting is enhanced under propofol, and enhanced thalamocortical feedback can strongly synchronize cortical UP states, then the cortical coordination needed for consciousness may be disrupted by too much synchrony within local cortical networks. Our model suggests that this occurs during peak-max, which happens more frequently at higher doses, and therefore this increase in local LFP-scale synchrony (as opposed to large-scale synchrony) may be responsible for the difference between arousable and unarousable propofol unconsciousness. At the same time, since ACh strengthens $\bar{g}_{\mathrm{AMPA:PY\rightarrow PY}}$, during high propofol doses, UP state synchrony may be more likely to spread between neighboring cortical columns, which may also explain the shift from arousable to unarousable unconsciousness under propofol. Finally, enhanced intracortical UP state synchrony during peak-max may also explain why peak-max coupling could extend to frequencies higher than alpha (Stephen et al. 2020) if higher frequency activity spreads more easily through these synchronized UP states. Ultimately, our model and the future work it guides may help to find the mechanistic difference between arousable and unarousable unconsciousness and, possibly, one cause of loss of consciousness.

Methods

bioRxiv preprint doi: https://doi.org/10.1101/2022.02.17.480766; this version posted February 20, 2022. The copyright holder for this preprint (which was not certified by peer review) is the author/funder, who has granted bioRxiv a license to display the preprint in perpetuity. It is made available under aCC-BY 4.0 International license.

Model Network Design

Our Hodgkin-Huxley network, illustrated in Figure 2 A, consists of 100 cortical pyramidal dendritic compartments (PYdr), 100 corresponding cortical pyramidal somatic/axonal compartments (PYso), 20 cortical interneuron cells (INs), 20 thalamic thalamocortical cells (TCs), and 20 thalamic reticular neurons (TRNs). All equations and parameters used in the model are available in both the Appendix and the model code (Soplata 2022b). The thalamic cells are identical to those used in (Soplata et al. 2017) and therefore derived from (Destexhe et al. 1996; Ching et al. 2010), except that we used a population size of 20 for each cell class rather than 50 due to memory/RAM limitations. All intrathalamic synapses between populations are all-to-all connected, just like in (Soplata et al. 2017). The cortical compartments and cells are implemented according to their original description in (Compte et al. 2003). For all cortical and thalamocortical synapses, each source cell is connected to (2*radius+1) target cells, where the radius is 10 cells. These connections overlap at the beginning and end of each cells for each population, and all synapses of a given source cell are equally weighted. Each PYdr compartment iss directly coupled to a single corresponding PYso compartment. While there are many slow models to choose from (Lytton, Destexhe, and Sejnowski 1996; Destexhe et al. 1996; Sanchez-Vives and McCormick 2000; Timofeev et al. 2000; Bazhenov et al. 2002; Destexhe and Sejnowski 2003; Hill and Tononi, Giulio 2004; V. Crunelli et al. 2011), we use this particular K(Na)-based sleep slow cortical model (Compte et al. 2003) due to its simplicity, experimental basis (Sanchez-Vives and McCormick 2000), and effective utilization in other slow models (Benita et al. 2012; Taxidis et al. 2013).

bioRxiv preprint doi: https://doi.org/10.1101/2022.02.17.480766; this version posted February 20, 2022. The copyright holder for this preprint (which was not certified by peer review) is the author/funder, who has granted bioRxiv a license to display the preprint in perpetuity. It is made available under aCC-BY 4.0 International license.

All connections are illustrated in Figure 2 A and available in both the Appendix and the model code (Soplata 2022b). AMPA connections include from PYso to neighbor-only PYdr (PYso→PYdr also called PY→PY), from PYso to IN (PY→IN), from TC to TRN (TC→TRN), from TC to PYdr (TC→PY), from TC to IN (TC→IN), from PYso to TRN (PY→TRN), and from PYso to TC (PY→TC). Intracortical AMPA connections (PYso→PYdr and PYso→IN) included synaptic depression. NMDA connections include from PYso to PYdr and from PYso to IN and include synaptic depression. $GABA_A$ connections include from IN to PYso (IN→PY), from IN to neighbor-only IN (IN→IN), from TRN to TC (TRN→TC), and from TRN to TRN (TRN→TRN). $GABA_B$ connections are only from TRN to TC (TC→TRN). Finally, simple compartmental connections exist between each PYdr and its corresponding PYso compartment. Note that we use PY→PY to refer exclusively to AMPAergic PYso→PYdr connections.

Propofol direct effects

Similarly to our previous work (Soplata et al. 2017), we model how increasing propofol directly affects the thalamocortical system via changing three parameters: decreasing TC cell H-current maximal conductance ($\bar{g}_H$), and potentiating all $GABA_A$ synapses via increasing maximal conductance ($\bar{g}_{GABA_A}$) and $GABA_A$ decay time constants (τ_{GABA_A}). Propofol may decrease $\bar{g}_H$ directly (Ying et al. 2006; Cacheaux et al. 2005), although the magnitude of this change is experimentally unknown (Chen 2005). To shift from a relay-mode state to a propofol-anesthetized state, we decrease $\bar{g}_H$ from 0.04 to 0.005 mS/cm^2, which is in line with previous anesthetic and sleep research using this thalamic model (Destexhe et al. 1996; Vijayan et al. 2013; Ching et al. 2010; Soplata et al. 2017).

bioRxiv preprint doi: https://doi.org/10.1101/2022.02.17.480766; this version posted February 20, 2022. The copyright holder for this preprint (which was not certified by peer review) is the author/funder, who has granted bioRxiv a license to display the preprint in perpetuity. It is made available under aCC-BY 4.0 International license.

For our propofol simulations, we triple $\bar{g}_{GABA_A}$ and τ_{GABA_A} for all $GABA_A$ synapses, since doubling these $GABA_A$ parameters did not effectively produce trough-max. We originally based the magnitude of our propofol $GABA_A$ changes on prior modeling work (McCarthy, Brown, and Kopell 2008). In our previous paper (Soplata et al. 2017), we found that our thalamus-only network could produce persistent alpha oscillations if we doubled or tripled these $GABA_A$ parameters. Importantly, in Figure 4 of (Soplata et al. 2017), we showed that thalamic persistent alpha occurred across a broader range of inputs when tripling the parameters compared to doubling. In the current paper, for all anesthetic simulation variations, doubling $GABA_A$ parameters produces very little simulation time of trough-max, instead producing peak-max, due to the lack of persistent thalamic alpha oscillations. Instead, only by tripling $GABA_A$ parameters do the simulations produce trough-max for a substantial or majority of simulation time. We suspect that cortical dynamics with lower doses of propofol require additional cortical cell types such as found in (McCarthy, Brown, and Kopell 2008). Since these cell types were not included in the model, we restrict our examination of cortical dynamics and its effects on thalamus to higher, anesthetic doses of propofol.

Propofol indirect effects (acetylcholine)

Propofol decreases cortical acetylcholine (ACh) (see Introduction), and we model these "indirect" anesthetic changes via increasing intracortical AMPAergic synaptic conductances ($\bar{g}_{AMPA:PY\rightarrow PY}$) (Compte et al. 2003; Benita et al. 2012; Krishnan et al. 2016), TC-to-PY thalamocortical AMPAergic synaptic conductances ($\bar{g}_{AMPA:TC\rightarrow PY}$) (Kruglikov and Rudy 2008;

bioRxiv preprint doi: https://doi.org/10.1101/2022.02.17.480766; this version posted February 20, 2022. The copyright holder for this preprint (which was not certified by peer review) is the author/funder, who has granted bioRxiv a license to display the preprint in perpetuity. It is made available under aCC-BY 4.0 International license.

Favero, Varghese, and Castro-Alamancos 2012), and K(Na)-current maximal conductance ($\bar{g}_{K(Na)}$) (Compte et al. 2003; Benita et al. 2012). ACh affects thalamocortical afferent synapses in different ways: decreased nicotinic ACh receptor activation weakens thalamocortical synapses, but decreased muscarinic ACh receptor activation strengthens them (Kruglikov and Rudy 2008; Favero, Varghese, and Castro-Alamancos 2012; Gil, Connors, and Amitai 1997; Hsieh, Cruikshank, and Metherate 2000; Oldford and Castro-Alamancos 2003; Eggermann and Feldmeyer 2009). Based on the rapid desensitization of nicotinic ACh receptors (Quick and Lester 2002), the slowly-changing, metabotropic nature of muscarinic receptors, and their similar shifts in natural sleep (McCormick 1992), we believe that muscarinic receptors could exert a stronger effect than nicotinic receptors on thalamocortical afferents, therefore increasing $\bar{g}_{AMPA:TC\rightarrow PY}$ with increasing propofol dose.

Dose parameters

For relay-mode, we apply none of the propofol effects and use the following parameters: $\bar{g}_{AMPA:PY\rightarrow PY}$ 0.004 mS/cm^2, $\bar{g}_{AMPA:TC\rightarrow PY}$ 0.004 mS/cm^2, TC $\bar{g}_H$ 0.04 mS/cm^2, PY $\bar{g}_{K(Na)}$ 0 mS/cm^2, and global $\bar{g}_{GABA_A}$ and τ_{GABA_A} modifier: 1x. We choose our relay-mode TC→PY and PY→PY maximal synaptic conductances (both 0.004 mS/cm^2) based on values slightly less than the value needed for one source cell spike to induce one target cell spike.

For direct-effects-only and all low-dose and high-dose propofol simulations, propofol direct effect parameters are as follows: TC $\bar{g}_H$ 0.005 mS/cm^2 and global $\bar{g}_{GABA_A}$ and τ_{GABA_A} modifier: 3x. We do not change propofol direct effect parameters between low- and high-dose propofol

bioRxiv preprint doi: https://doi.org/10.1101/2022.02.17.480766; this version posted February 20, 2022. The copyright holder for this preprint (which was not certified by peer review) is the author/funder, who has granted bioRxiv a license to display the preprint in perpetuity. It is made available under aCC-BY 4.0 International license.

because only tripling rather than doubling $GABA_A$ parameters enabled trough-max (see previous section *Propofol direct effects*) and further changes to $\bar{g}_H$ may have changed the frequency and susceptibility of thalamic alpha when our primary aim was to investigate how thalamic alpha interacts with cortical slow coupling.

For low-dose propofol simulations, corresponding to indirect effects, we increase PY $\bar{g}_{K(Na)}$ to 1.33 mS/cm^2, $\bar{g}_{\mathrm{AMPA:TC\rightarrow PY}}$ to 0.005 mS/cm^2 and $\bar{g}_{\mathrm{AMPA:PY\rightarrow PY}}$ to 0.0075 mS/cm^2, while for high-dose simulations, we further increase PY $\bar{g}_{K(Na)}$ to 1.5 mS/cm^2 and both $\bar{g}_{\mathrm{AMPA:TC\rightarrow PY}}$ and $\bar{g}_{\mathrm{AMPA:PY\rightarrow PY}}$ to 0.01 mS/cm^2. Low- and high-dose values of PY $\bar{g}_{K(Na)}$ were used for their similarity to slow investigations with the original model (Benita et al. 2012). Different computational models use a range of proportional increases to $\bar{g}_{\mathrm{AMPA:PY\rightarrow PY}}$ caused by ACh, including up to +75% (Vijayan et al. 2013) or +15% to +100% (Krishnan et al. 2016). Data on how much ACh may increase $\bar{g}_{\mathrm{AMPA:TC\rightarrow PY}}$ is much more scarce, but the increase may be as high as +300% (see Figure 8 F of (Favero, Varghese, and Castro-Alamancos 2012)). However, the effect of these ACh changes on the system may be even more pronounced due to the large differences in intracortical and thalamocortical maximal AMPAergic conductance assumptions, which can span more than an order of magnitude of difference just between biophysical models alone (Traub et al. 2005; Ching et al. 2010; Vijayan et al. 2013; Krishnan et al. 2016). Based on our initial relay-mode $\bar{g}_{\mathrm{AMPA:PY\rightarrow PY}}$ and $\bar{g}_{\mathrm{AMPA:TC\rightarrow PY}}$ values of 0.004 mS/cm^2, we limit our analysis to the extensive network changes that occur within +150% of these values to try to stay as close to biological realism as possible. The only exception to this is where we increase each indirect effect to its corresponding high-dose level by itself (given above) but kept all other values at low-dose conditions.

bioRxiv preprint doi: https://doi.org/10.1101/2022.02.17.480766; this version posted February 20, 2022. The copyright holder for this preprint (which was not certified by peer review) is the author/funder, who has granted bioRxiv a license to display the preprint in perpetuity. It is made available under aCC-BY 4.0 International license.

LFP Model

For our LFP model and PAC analysis, we rely on the total combined cortical AMPAergic synaptic currents of TC→PY and PY→PY synapses, in units of $\mu A/cm^2$, except when otherwise indicated to look at individual synapse types. We base this analysis on the assumption that the primary determinants of LFP, like most electrode signals, are local excitatory synaptic currents (Nunez and Srinivasan 2006; Buzsáki, Anastassiou, and Koch 2012; Einevoll et al. 2013).

Coupling Analysis

For the comodulograms of the LFP signals, we use the Modulation Index method (Tort et al. 2010) as implemented in MATLAB by Angela Onslow (Onslow, Bogacz, and Jones 2011) to estimate phase-amplitude coupling in Figure 7 and Figure 9. A copy of this analysis software is available in the modified DynaSim toolbox used for this work (Soplata 2022a) , and the parameters used for each analysis are available online in the script files used to run the simulations and analysis (Soplata 2022b).

Simulations and Reproducibility

All of the simulation parameters (Soplata 2022b) and model code (Soplata 2022c) needed to reproduce the simulations shown in this work are available online on GitHub. All simulations were run using a custom version (Soplata 2022a) of the MATLAB simulation toolbox DynaSim

bioRxiv preprint doi: https://doi.org/10.1101/2022.02.17.480766; this version posted February 20, 2022. The copyright holder for this preprint (which was not certified by peer review) is the author/funder, who has granted bioRxiv a license to display the preprint in perpetuity. It is made available under aCC-BY 4.0 International license.

(Sherfey et al. 2018) located online. Individual simulations should be reproducible on a modern desktop computer with access to RAM of 32 gigglebytes or higher.

Human Data for Figure 1

Human experimental data used in Figure 1 is from a single subject analyzed in (Purdon et al. 2013) and subject to the same methodology and analysis.

Appendix:

Equations for Computational Models (attached as PDF)

Acknowledgements:

The authors would like to thank Jason Sherfey, Erik A. Roberts, and Caroline Moore-Kochlacs for their suggestions during the investigation.

Grants:

All authors were supported by NIH Grant P01GM118269. Other sources include Guggenheim Fellowship in Applied Mathematics, NIH R01-GM104948, funds from MGH, and NSF DMS-1042134-5.

Disclosures:

Massachusetts General Hospital has licensed intellectual property for EEG monitoring developed by Drs. Brown and Purdon to Masimo Corporation. Drs. Brown and Purdon hold interests in, and

bioRxiv preprint doi: https://doi.org/10.1101/2022.02.17.480766; this version posted February 20, 2022. The copyright holder for this preprint (which was not certified by peer review) is the author/funder, who has granted bioRxiv a license to display the preprint in perpetuity. It is made available under aCC-BY 4.0 International license.

Dr. Purdon is a co-founder of, PASACALL Systems, Inc., a start-up company developing EEG-based anesthetic state control systems for anesthesiology.

Supplementals:

Supplemental Data 1. Simulation PAC data, available at

https://doi.org/10.6084/m9.figshare.19175720.v1

Endnote:

At the request of the author(s), readers are herein alerted to the fact that additional materials related to this manuscript ("Ancillary Information 1") may be found at https://doi.org/10.6084/m9.figshare.19184564 . These materials are not a part of this manuscript and have not undergone peer review by the American Physiological Society (APS). APS and the journal editors take no responsibility for these materials, for the website address, or for any links to or from it.

bioRxiv preprint doi: https://doi.org/10.1101/2022.02.17.480766; this version posted February 20, 2022. The copyright holder for this preprint (which was not certified by peer review) is the author/funder, who has granted bioRxiv a license to display the preprint in perpetuity. It is made available under aCC-BY 4.0 International license.

References

Amzica, Florin, and Mircea Steriade. 2002. "The Functional Significance of K-Complexes." *Sleep Medicine Reviews* 6 (2): 139–49. https://doi.org/10.1053/smrv.2001.0181.

Banks, Matthew I., Bryan M. Krause, Christopher M. Endemann, Declan I. Campbell, Christopher K. Kovach, Mark Eric Dyken, Hiroto Kawasaki, and Kirill V. Nourski. 2020. "Cortical Functional Connectivity Indexes Arousal State during Sleep and Anesthesia." *NeuroImage* 211 (May): 116627. https://doi.org/10.1016/j.neuroimage.2020.116627.

Bazhenov, Maxim, Igor Timofeev, Mircea Steriade, and Terrence J Sejnowski. 2002. "Model of Thalamocortical Slow-Wave Sleep Oscillations and Transitions to Activated States." *The Journal of Neuroscience : The Official Journal of the Society for Neuroscience*. 22 (19): 8691–8704. https://doi.org/10.1523/JNEUROSCI.22-19-08691.2002.

Benita, Jose M., Antoni Guillamon, Gustavo Deco, and Maria V. Sanchez-Vives. 2012. "Synaptic Depression and Slow Oscillatory Activity in a Biophysical Network Model of the Cerebral Cortex." *Frontiers in Computational Neuroscience* 6. https://doi.org/10.3389/fncom.2012.00064.

Brown, Emery N., Ralph Lydic, and Nicholas D. Schiff. 2010. "General Anesthesia, Sleep, and Coma." *The New England Journal of Medicine* 363 (27): 2638–50. https://doi.org/10.1056/nejmra0808281.

Brown, Emery N., Patrick L. Purdon, and Christa J. Van Dort. 2011. "General Anesthesia and Altered States of Arousal: A Systems Neuroscience Analysis." *Annual Review of Neuroscience* 34 (1): 601–28. https://doi.org/10.1146/annurev-neuro-060909-153200.

bioRxiv preprint doi: https://doi.org/10.1101/2022.02.17.480766; this version posted February 20, 2022. The copyright holder for this preprint (which was not certified by peer review) is the author/funder, who has granted bioRxiv a license to display the preprint in perpetuity. It is made available under aCC-BY 4.0 International license.

Buzsáki, György, Costas A. Anastassiou, and Christof Koch. 2012. "The Origin of Extracellular Fields and Currents — EEG, ECoG, LFP and Spikes." *Nature Reviews Neuroscience* 13 (6): 407–20. https://doi.org/10.1038/nrn3241.

Cacheaux, L. P., Norbert Topf, Gareth R. Tibbs, Ulrich R. Schaefer, Roberto Levi, Neil L. Harrison, Geoffrey W. Abbott, and Peter A. Goldstein. 2005. "Impairment of Hyperpolarization-Activated, Cyclic Nucleotide-Gated Channel Function by the Intravenous General Anesthetic Propofol." *The Journal of Pharmacology and Experimental Therapeutics* 315 (2): 517–25. https://doi.org/10.1124/jpet.105.091801.

Cash, S. S., E. Halgren, N. Dehghani, A. O. Rossetti, T. Thesen, C. Wang, O. Devinsky, et al. 2009. "The Human K-Complex Represents an Isolated Cortical Down-State." *Science* 324 (5930): 1084–87. https://doi.org/10.1126/science.1169626.

Chen, X. 2005. "HCN Subunit-Specific and CAMP-Modulated Effects of Anesthetics on Neuronal Pacemaker Currents." *Journal of Neuroscience* 25 (24): 5803–14. https://doi.org/10.1523/JNEUROSCI.1153-05.2005.

Ching, S., A. Cimenser, P. L. Purdon, E. N. Brown, and N. J. Kopell. 2010. "Thalamocortical Model for a Propofol-Induced Alpha-Rhythm Associated with Loss of Consciousness." *Proceedings of the National Academy of Sciences of the United States of America* 107 (52): 22665–70. https://doi.org/10.1073/pnas.1017069108.

Ching, S., P. L. Purdon, S. Vijayan, N. J. Kopell, and E. N. Brown. 2012. "A Neurophysiological-Metabolic Model for Burst Suppression." *Proceedings of the National Academy of Sciences of the United States of America* 109 (8): 3095–3100. https://doi.org/10.1073/pnas.1121461109.

bioRxiv preprint doi: https://doi.org/10.1101/2022.02.17.480766; this version posted February 20, 2022. The copyright holder for this preprint (which was not certified by peer review) is the author/funder, who has granted bioRxiv a license to display the preprint in perpetuity. It is made available under aCC-BY 4.0 International license.

Cimenser, A., P. L. Purdon, E. T. Pierce, J. L. Walsh, A. F. Salazar-Gomez, P. G. Harrell, C. Tavares-Stoeckel, K. Habeeb, and E. N. Brown. 2011. "Tracking Brain States under General Anesthesia by Using Global Coherence Analysis." *Proceedings of the National Academy of Sciences* 108 (21): 8832–37. https://doi.org/10.1073/pnas.1017041108.

Compte, Albert, Maria V. Sanchez-Vives, David A. McCormick, and Xiao-Jing Wang. 2003. "Cellular and Network Mechanisms of Slow Oscillatory Activity (<1 Hz) and Wave Propagations in a Cortical Network Model." *Journal of Neurophysiology* 89 (5): 2707–25. https://doi.org/10.1152/jn.00845.2002.

Crunelli, V., A. C. Errington, S. W. Hughes, and T. I. Toth. 2011. "The Thalamic Low-Threshold Ca2+ Potential: A Key Determinant of the Local and Global Dynamics of the Slow (<1 Hz) Sleep Oscillation in Thalamocortical Networks." *Philosophical Transactions of the Royal Society of London. A* 369 (1952): 3820–39. https://doi.org/10.1098/rsta.2011.0126.

Crunelli, Vincenzo, and Stuart W Hughes. 2010. "The Slow (<1 Hz) Rhythm of Non-REM Sleep: A Dialogue between Three Cardinal Oscillators." *Nature Neuroscience* 13 (1): 9–17. https://doi.org/10.1038/nn.2445.

Cunningham, M. O., D. D. Pervouchine, C. Racca, N. J. Kopell, C. H. Davies, R. S. G. Jones, R. D. Traub, and M. A. Whittington. 2006. "Neuronal Metabolism Governs Cortical Network Response State." *Proceedings of the National Academy of Sciences* 103 (14): 5597–5601.

Destexhe, Alain, Thierry Bal, David A. McCormick, and Terrence J. Sejnowski. 1996. "Ionic Mechanisms Underlying Synchronized Oscillations and Propagating Waves in a Model

bioRxiv preprint doi: https://doi.org/10.1101/2022.02.17.480766; this version posted February 20, 2022. The copyright holder for this preprint (which was not certified by peer review) is the author/funder, who has granted bioRxiv a license to display the preprint in perpetuity. It is made available under aCC-BY 4.0 International license.

of Ferret Thalamic Slices." *Journal of Neurophysiology* 76 (3): 2049–70. https://doi.org/10.1152/jn.1996.76.3.2049.

Destexhe, Alain, and T. J. Sejnowski. 2003. "Interactions between Membrane Conductances Underlying Thalamocortical Slow-Wave Oscillations." *Physiological Reviews* 83 (4): 1401–53. https://doi.org/10.1152/physrev.00012.2003.

Eggermann, Emmanuel, and Dirk Feldmeyer. 2009. "Cholinergic Filtering in the Recurrent Excitatory Microcircuit of Cortical Layer 4." *Proceedings of the National Academy of Sciences* 106 (28): 11753–58. https://doi.org/10.1073/pnas.0810062106.

Einevoll, Gaute T., Christoph Kayser, Nikos K. Logothetis, and Stefano Panzeri. 2013. "Modelling and Analysis of Local Field Potentials for Studying the Function of Cortical Circuits." *Nature Reviews Neuroscience* 14 (11): 770–85. https://doi.org/10.1038/nrn3599.

Favero, Morgana, Gladis Varghese, and Manuel A Castro-Alamancos. 2012. "The State of Somatosensory Cortex during Neuromodulation." *Journal of Neurophysiology* 108 (4): 1010–24. https://doi.org/10.1152/jn.00256.2012.

Flores, Francisco J., Katharine E. Hartnack, Amanda B. Fath, Seong-Eun Kim, Matthew A. Wilson, Emery N. Brown, and Patrick L. Purdon. 2017. "Thalamocortical Synchronization during Induction and Emergence from Propofol-Induced Unconsciousness." *Proceedings of the National Academy of Sciences of the United States of America* 114 (32): E6660–68. https://doi.org/10.1073/pnas.1700148114.

Galarza Vallejo, Ana, Marijn C W Kroes, Enrique Rey, Maria Victoria Acedo, Stephan Moratti, Guillén Fernández, and Bryan A Strange. 2019. "Propofol-Induced Deep Sedation

bioRxiv preprint doi: https://doi.org/10.1101/2022.02.17.480766; this version posted February 20, 2022. The copyright holder for this preprint (which was not certified by peer review) is the author/funder, who has granted bioRxiv a license to display the preprint in perpetuity. It is made available under aCC-BY 4.0 International license.

Reduces Emotional Episodic Memory Reconsolidation in Humans." *Science Advances* 5 (3): eaav3801. https://doi.org/10.1126/sciadv.aav3801.

Gaskell, A. L., D. F. Hight, J. Winders, G. Tran, A. Defresne, V. Bonhomme, A. Raz, J. W. Sleigh, and R. D. Sanders. 2017. "Frontal Alpha-Delta EEG Does Not Preclude Volitional Response during Anaesthesia: Prospective Cohort Study of the Isolated Forearm Technique." *British Journal of Anaesthesia*, August. https://doi.org/10.1093/bja/aex170.

Gemignani, Angelo, Danilo Menicucci, Marco Laurino, Andrea Piarulli, Francesca Mastorci, Laura Sebastiani, and Paolo Allegrini. 2015. "Linking Sleep Slow Oscillations with Consciousness Theories: New Vistas on Slow Wave Sleep Unconsciousness." *Archives Italiennes de Biologie* 153 (2–3): 135–43. https://doi.org/10.4449/aib.v153i2-3.4041.

Gil, Ziv, Barry W Connors, and Yael Amitai. 1997. "Differential Regulation of Neocortical Synapses by Neuromodulators and Activity." *Neuron* 19 (3): 679–86. https://doi.org/10.1016/S0896-6273(00)80380-3.

Gutiérrez, Rodrigo, Felipe Maldonado, Jose I. Egaña, and Antonello Penna. 2022. "Electroencephalographic Alpha and Delta Oscillation Dynamics in Response to Increasing Doses of Propofol." *Journal of Neurosurgical Anesthesiology* 34 (1): 79–83. https://doi.org/10.1097/ANA.0000000000000733.

Hage, Travis A, and Lawrence Salkoff. 2012. "Sodium-Activated Potassium Channels Are Functionally Coupled to Persistent Sodium Currents." *The Journal of Neuroscience: The Official Journal of the Society for Neuroscience.* 32 (8): 2714–21. https://doi.org/10.1523/JNEUROSCI.5088-11.2012.

bioRxiv preprint doi: https://doi.org/10.1101/2022.02.17.480766; this version posted February 20, 2022. The copyright holder for this preprint (which was not certified by peer review) is the author/funder, who has granted bioRxiv a license to display the preprint in perpetuity. It is made available under aCC-BY 4.0 International license.

Hill, S. and Tononi, Giulio. 2004. "Modeling Sleep and Wakefulness in the Thalamocortical System." *Journal of Neurophysiology* 93 (3): 1671–98. https://doi.org/10.1152/jn.00915.2004.

Hsieh, C Y, S J Cruikshank, and R Metherate. 2000. "Differential Modulation of Auditory Thalamocortical and Intracortical Synaptic Transmission by Cholinergic Agonist." *Brain Res.* 880 (1–2): 51–64.

Hudetz, Anthony G., and George A. Mashour. 2016. "Disconnecting Consciousness: Is There a Common Anesthetic End Point?" *Anesthesia & Analgesia* 123 (5): 1228–40. https://doi.org/10.1213/ANE.0000000000001353.

Kikuchi, T, Y Wang, K Sato, and F Okumura. 1998. "In Vivo Effects of Propofol on Acetylcholine Release from the Frontal Cortex, Hippocampus and Striatum Studied by Intracerebral Microdialysis in Freely Moving Rats." *British Journal of Anaesthesia* 80 (5): 644–48. https://doi.org/10.1093/bja/80.5.644.

Krishnan, Giri P., Sylvain Chauvette, Isaac Shamie, Sara Soltani, Igor Timofeev, Sydney S. Cash, Eric Halgren, and Maxim Bazhenov. 2016. "Cellular and Neurochemical Basis of Sleep Stages in the Thalamocortical Network." *ELife* 5: e18607. https://doi.org/10.7554/eLife.18607.

Krom, Aaron J., Amit Marmelshtein, Hagar Gelbard-Sagiv, Ariel Tankus, Hanna Hayat, Daniel Hayat, Idit Matot, et al. 2020. "Anesthesia-Induced Loss of Consciousness Disrupts Auditory Responses beyond Primary Cortex." *Proceedings of the National Academy of Sciences*, May. https://doi.org/10.1073/pnas.1917251117.

bioRxiv preprint doi: https://doi.org/10.1101/2022.02.17.480766; this version posted February 20, 2022. The copyright holder for this preprint (which was not certified by peer review) is the author/funder, who has granted bioRxiv a license to display the preprint in perpetuity. It is made available under aCC-BY 4.0 International license.

Kruglikov, Illya, and Bernardo Rudy. 2008. "Perisomatic GABA Release and Thalamocortical Integration onto Neocortical Excitatory Cells Are Regulated by Neuromodulators." *Neuron* 58 (6): 911–24. https://doi.org/10.1016/j.neuron.2008.04.024.

Kuo, Min-Ching, and Hans C. Dringenberg. 2008. "Histamine Facilitates in Vivo Thalamocortical Long-Term Potentiation in the Mature Visual Cortex of Anesthetized Rats." *European Journal of Neuroscience* 27 (7): 1731–38. https://doi.org/10.1111/j.1460-9568.2008.06164.x.

Lee, Minji, Robert D. Sanders, Seul-Ki Yeom, Dong-Ok Won, Kwang-Suk Seo, Hyun Jeong Kim, Giulio Tononi, and Seong-Whan Lee. 2017. "Network Properties in Transitions of Consciousness during Propofol-Induced Sedation." *Scientific Reports* 7 (1): 16791. https://doi.org/10.1038/s41598-017-15082-5.

Luo, Tian-Yuan, Shuang Cai, Zai-Xun Qin, Shao-Cheng Yang, Yue Shu, Cheng-Xi Liu, Yu Zhang, et al. 2020. "Basal Forebrain Cholinergic Activity Modulates Isoflurane and Propofol Anesthesia." *Frontiers in Neuroscience* 14: 1086. https://doi.org/10.3389/fnins.2020.559077.

Lytton, W. W., A. Destexhe, and T. J. Sejnowski. 1996. "Control of Slow Oscillations in the Thalamocortical Neuron: A Computer Model." *The Journal of Neuroscience□: The Official Journal of the Society for Neuroscience*. 70 (3): 673–84. https://doi.org/10.1016/S0306-4522(96)83006-5.

Malekmohammadi, Mahsa, Collin M. Price, Andrew E. Hudson, Jasmine A. T. DiCesare, and Nader Pouratian. 2019. "Propofol-Induced Loss of Consciousness Is Associated with a Decrease in Thalamocortical Connectivity in Humans." *Brain*. https://doi.org/10.1093/brain/awz169.

bioRxiv preprint doi: https://doi.org/10.1101/2022.02.17.480766; this version posted February 20, 2022. The copyright holder for this preprint (which was not certified by peer review) is the author/funder, who has granted bioRxiv a license to display the preprint in perpetuity. It is made available under aCC-BY 4.0 International license.

McCarthy, Michelle M., Emery N. Brown, and Nancy Kopell. 2008. "Potential Network Mechanisms Mediating Electroencephalographic Beta Rhythm Changes during Propofol-Induced Paradoxical Excitation." *The Journal of Neuroscience : The Official Journal of the Society for Neuroscience.* 28 (50): 13488–504. https://doi.org/10.1523/JNEUROSCI.3536-08.2008.

McCormick, David A. 1992. "Neurotransmitter Actions in the Thalamus and Cerebral Cortex and Their Role in Neuromodulation of Thalamocortical Activity." *Progress in Neurobiology* 39 (4): 337–88. https://doi.org/10.1016/0301-0082(92)90012-4.

Meuret, P., S. B. Backman, V. Bonhomme, G. Plourde, and P. Fiset. 2000. "Physostigmine Reverses Propofol-Induced Unconsciousness and Attenuation of the Auditory Steady State Response and Bispectral Index in Human Volunteers." *Anesthesiology* 93 (3): 708–17.

Mhuircheartaigh, Róisín Ní, Catherine Warnaby, Richard Rogers, Saad Jbabdi, and Irene Tracey. 2013. "Slow-Wave Activity Saturation and Thalamocortical Isolation during Propofol Anesthesia in Humans." *Science Translational Medicine* 5 (208): 208ra148-208ra148.

Minert, Anne, Mark Baron, and Marshall Devor. 2020. "Reduced Sensitivity to Anesthetic Agents upon Lesioning the Mesopontine Tegmental Anesthesia Area in Rats Depends on Anesthetic Type." *Anesthesiology* 132 (3): 535–50. https://doi.org/10.1097/ALN.0000000000003087.

Minert, Anne, Shai-Lee Yatziv, and Marshall Devor. 2017. "Location of the Mesopontine Neurons Responsible for Maintenance of Anesthetic Loss of Consciousness." *Journal of Neuroscience* 37 (38): 9320–31. https://doi.org/10.1523/JNEUROSCI.0544-17.2017.

bioRxiv preprint doi: https://doi.org/10.1101/2022.02.17.480766; this version posted February 20, 2022. The copyright holder for this preprint (which was not certified by peer review) is the author/funder, who has granted bioRxiv a license to display the preprint in perpetuity. It is made available under aCC-BY 4.0 International license.

Moody, Olivia A., Edlyn R. Zhang, Kathleen F. Vincent, Risako Kato, Eric D. Melonakos, Christa J. Nehs, and Ken Solt. 2021. "The Neural Circuits Underlying General Anesthesia and Sleep." *Anesthesia & Analgesia* 132 (5): 1254–64. https://doi.org/10.1213/ANE.0000000000005361.

Morrison, John H., and Mark G. Baxter. 2012. "The Aging Cortical Synapse: Hallmarks and Implications for Cognitive Decline." *Nature Reviews Neuroscience* 13 (4): 240–50. https://doi.org/10.1038/nrn3200.

Muindi, Fanuel, Jonathan D. Kenny, Norman E. Taylor, Ken Solt, Matthew A. Wilson, Emery N. Brown, and Christa J. Van Dort. 2016. "Electrical Stimulation of the Parabrachial Nucleus Induces Reanimation from Isoflurane General Anesthesia." *Behavioural Brain Research* 306 (June): 20–25. https://doi.org/10.1016/j.bbr.2016.03.021.

Mukamel, E. A., E. Pirondini, B. Babadi, K. F. K. Wong, E. T. Pierce, P. G. Harrell, J. L. Walsh, et al. 2014. "A Transition in Brain State during Propofol-Induced Unconsciousness." *The Journal of Neuroscience : The Official Journal of the Society for Neuroscience.* 34 (3): 839–45. https://doi.org/10.1523/JNEUROSCI.5813-12.2014.

Nemoto, Chiaki, Masahiro Murakawa, Takahiro Hakozaki, Tuyoshi Imaizumi, Tuyoshi Isosu, and Shinju Obara. 2013. "Effects of Dexmedetomidine, Midazolam, and Propofol on Acetylcholine Release in the Rat Cerebral Cortex in Vivo." *Journal of Anesthesia* 27 (5): 771–74. https://doi.org/10.1007/s00540-013-1589-5.

Neske, Garrett T. 2016. "The Slow Oscillation in Cortical and Thalamic Networks: Mechanisms and Functions." *Frontiers in Neural Circuits* 9 (January). https://doi.org/10.3389/fncir.2015.00088.

bioRxiv preprint doi: https://doi.org/10.1101/2022.02.17.480766; this version posted February 20, 2022. The copyright holder for this preprint (which was not certified by peer review) is the author/funder, who has granted bioRxiv a license to display the preprint in perpetuity. It is made available under aCC-BY 4.0 International license.

Nunez, Paul L., and Ramesh Srinivasan. 2006. *Electric Fields of the Brain: The Neurophysics of EEG*. 2nd ed. Oxford□; New York: Oxford University Press.

Oldford, E, and M. A Castro-Alamancos. 2003. "Input-Specific Effects of Acetylcholine on Sensory and Intracortical Evoked Responses in the 'Barrel Cortex' in Vivo." *Neuroscience* 117 (3): 769–78. https://doi.org/10.1016/S0306-4522(02)00663-2.

Onslow, Angela C.E., Rafal Bogacz, and Matthew W. Jones. 2011. "Quantifying Phase–Amplitude Coupling in Neuronal Network Oscillations." *Progress in Biophysics and Molecular Biology* 105 (1–2): 49–57. https://doi.org/10.1016/j.pbiomolbio.2010.09.007.

Pal, Dinesh, and George A. Mashour. 2021. "Consciousness, Anesthesia, and Acetylcholine." *Anesthesiology* 134 (4): 515–17. https://doi.org/10.1097/ALN.0000000000003696.

Palva, Satu, and J. Matias Palva. 2007. "New Vistas for α-Frequency Band Oscillations." *Trends in Neurosciences* 30 (4): 150–58. https://doi.org/10.1016/j.tins.2007.02.001.

Penagos, Hector, Carmen Varela, and Matthew A Wilson. 2017. "Oscillations, Neural Computations and Learning during Wake and Sleep." *Current Opinion in Neurobiology* 44 (June): 193–201. https://doi.org/10.1016/j.conb.2017.05.009.

Peters, Alan. 2002. "Structural Changes That Occur during Normal Aging of Primate Cerebral Hemispheres." *Neuroscience and Biobehavioral Reviews* 26 (7): 733–41. https://doi.org/10.1016/S0149-7634(02)00060-X.

Purdon, P. L., K. J. Pavone, O. Akeju, A. C. Smith, A. L. Sampson, J. Lee, D. W. Zhou, K. Solt, and E. N. Brown. 2015. "The Ageing Brain: Age-Dependent Changes in the Electroencephalogram during Propofol and Sevoflurane General Anaesthesia." *British Journal of Anaesthesia* 115 (Suppl 1): i46–57. https://doi.org/10.1093/bja/aev213.

bioRxiv preprint doi: https://doi.org/10.1101/2022.02.17.480766; this version posted February 20, 2022. The copyright holder for this preprint (which was not certified by peer review) is the author/funder, who has granted bioRxiv a license to display the preprint in perpetuity. It is made available under aCC-BY 4.0 International license.

Purdon, P. L., E. T. Pierce, E. A. Mukamel, M. J. Prerau, J. L. Walsh, K. F. K. Wong, A. F. Salazar-Gomez, et al. 2013. "Electroencephalogram Signatures of Loss and Recovery of Consciousness from Propofol." *Proceedings of the National Academy of Sciences of the United States of America* 110 (12): E1142–51. https://doi.org/10.1073/pnas.1221180110.

Quick, Michael W., and Robin A. J. Lester. 2002. "Desensitization of Neuronal Nicotinic Receptors." *Journal of Neurobiology* 53 (4): 457–78. https://doi.org/10.1002/neu.10109.

Redinbaugh, Michelle J., Jessica M. Phillips, Niranjan A. Kambi, Sounak Mohanta, Samantha Andryk, Gaven L. Dooley, Mohsen Afrasiabi, Aeyal Raz, and Yuri B. Saalmann. 2020. "Thalamus Modulates Consciousness via Layer-Specific Control of Cortex." *Neuron* 106 (1): 66-75.e12. https://doi.org/10.1016/j.neuron.2020.01.005.

Sanchez-Vives, Maria V., and David A. McCormick. 2000. "Cellular and Network Mechanisms of Rhythmic Recurrent Activity in Neocortex." *Nature Neuroscience* 3 (10): 1027–34.

Sanchez-Vives, Maria V., Lionel G. Nowak, and David A. McCormick. 2000. "Cellular Mechanisms of Long-Lasting Adaptation in Visual Cortical Neurons In Vitro." *The Journal of Neuroscience : The Official Journal of the Society for Neuroscience.* 20 (11): 4286–99. https://doi.org/10.1523/JNEUROSCI.20-11-04286.2000.

Schwindt, P C, W J Spain, and W E Crill. 1989. "Long-Lasting Reduction of Excitability by a Sodium-Dependent Potassium Current in Cat Neocortical Neurons." *Journal of Neurophysiology* 61 (2): 233–44. https://doi.org/10.1152/jn.1989.61.2.233.

Sherfey, Jason S., Austin E. Soplata, Salva Ardid, Erik A. Roberts, David A. Stanley, Benjamin R. Pittman-Polletta, and Nancy J. Kopell. 2018. "DynaSim: A MATLAB Toolbox for Neural Modeling and Simulation." *Frontiers in Neuroinformatics* 12. https://doi.org/10.3389/fninf.2018.00010.

bioRxiv preprint doi: https://doi.org/10.1101/2022.02.17.480766; this version posted February 20, 2022. The copyright holder for this preprint (which was not certified by peer review) is the author/funder, who has granted bioRxiv a license to display the preprint in perpetuity. It is made available under aCC-BY 4.0 International license.

Soplata, Austin E. 2022a. *Dynasim Fork for Soplata 2022*. https://github.com/asoplata/DynaSim/tree/coupling_addition.

———. 2022b. *Full Soplata 2022 Code*. https://github.com/asoplata/soplata-2022-thalcort-code.

———. 2022c. *Mechanism Code for Soplata 2022 Model*. MATLAB. https://github.com/asoplata/dynasim-extended-benita-model.

Soplata, Austin E., Michelle M. McCarthy, Jason Sherfey, Shane Lee, Patrick L. Purdon, Emery N. Brown, and Nancy Kopell. 2017. "Thalamocortical Control of Propofol Phase-Amplitude Coupling." *PLoS Computational Biology* 13 (12): e1005879. https://doi.org/10.1371/journal.pcbi.1005879.

Stephen, Emily P., Gladia C. Hotan, Eric T. Pierce, P. Grace Harrell, John L. Walsh, Emery N. Brown, and Patrick L. Purdon. 2020. "Broadband Slow-Wave Modulation in Posterior and Anterior Cortex Tracks Distinct States of Propofol-Induced Unconsciousness." *Scientific Reports* 10 (1): 13701. https://doi.org/10.1038/s41598-020-68756-y.

Stickgold, Robert. 2005. "Sleep-Dependent Memory Consolidation." *Nature* 437 (7063): 1272–78. https://doi.org/10.1038/nature04286.

Taxidis, Jiannis, Kenji Mizuseki, Robert Mason, and Markus R. Owen. 2013. "Influence of Slow Oscillation on Hippocampal Activity and Ripples through Cortico-Hippocampal Synaptic Interactions, Analyzed by a Cortical-CA3-CA1 Network Model." *Frontiers in Computational Neuroscience* 7. https://doi.org/10.3389/fncom.2013.00003.

Timofeev, I., F. Grenier, M. Bazhenov, T. J. Sejnowski, and M. Steriade. 2000. "Origin of Slow Cortical Oscillations in Deafferented Cortical Slabs." *Cerebral Cortex (New York, N.Y.: 1991)* 10 (12): 1185–99. https://doi.org/10.1093/cercor/10.12.1185.

bioRxiv preprint doi: https://doi.org/10.1101/2022.02.17.480766; this version posted February 20, 2022. The copyright holder for this preprint (which was not certified by peer review) is the author/funder, who has granted bioRxiv a license to display the preprint in perpetuity. It is made available under aCC-BY 4.0 International license.

Tinker, John H., Frank W. Sharbrough, and John D. Michenfelder. 1977. "Anterior Shift of the Dominant EEG Rhythm during Anesthesia in the Java Monkey: Correlation with Anesthetic Potency." *Anesthesiology*.

Tort, A. B. L., R. Komorowski, H. Eichenbaum, and N. Kopell. 2010. "Measuring Phase-Amplitude Coupling Between Neuronal Oscillations of Different Frequencies." *Journal of Neurophysiology* 104 (2): 1195–1210. https://doi.org/10.1152/jn.00106.2010.

Traub, Roger D, Diego Contreras, Mark O Cunningham, Hilary Murray, Fiona E N LeBeau, Anita Roopun, Andrea Bibbig, W Bryan Wilent, Michael J Higley, and Miles A Whittington. 2005. "Single-Column Thalamocortical Network Model Exhibiting Gamma Oscillations, Sleep Spindles, and Epileptogenic Bursts." *J. Neurophysiol.* 93 (4): 2194–2232.

Vijayan, S., S. Ching, P. L. Purdon, E. N. Brown, and N. J. Kopell. 2013. "Thalamocortical Mechanisms for the Anteriorization of Alpha Rhythms during Propofol-Induced Unconsciousness." *The Journal of Neuroscience : The Official Journal of the Society for Neuroscience.* 33 (27): 11070–75. https://doi.org/10.1523/JNEUROSCI.5670-12.2013.

Vlasov, Ksenia, JunZhu Pei, Christa J. Nehs, Jennifer A. Guidera, Edlyn R. Zhang, Jonathan D. Kenny, Timothy T. Houle, Gary J. Brenner, Norman E. Taylor, and Ken Solt. 2021. "Activation of GABAergic Neurons in the Rostromedial Tegmental Nucleus and Other Brainstem Regions Promotes Sedation and Facilitates Sevoflurane Anesthesia in Mice." *Anesthesia & Analgesia* 132 (4): e50. https://doi.org/10.1213/ANE.0000000000005387.

Ying, Shui-Wang, Syed Y. Abbas, Neil L. Harrison, and Peter A. Goldstein. 2006. "Propofol Block of Ih Contributes to the Suppression of Neuronal Excitability and Rhythmic Burst Firing in Thalamocortical Neurons: Propofol Inhibition of Thalamic Ih." *The European*

bioRxiv preprint doi: https://doi.org/10.1101/2022.02.17.480766; this version posted February 20, 2022. The copyright holder for this preprint (which was not certified by peer review) is the author/funder, who has granted bioRxiv a license to display the preprint in perpetuity. It is made available under aCC-BY 4.0 International license.

Journal of Neuroscience 23 (2): 465–80. https://doi.org/10.1111/j.1460-9568.2005.04587.x.

bioRxiv preprint doi: https://doi.org/10.1101/2022.02.17.480766; this version posted February 20, 2022. The copyright holder for this preprint (which was not certified by peer review) is the author/funder, who has granted bioRxiv a license to display the preprint in perpetuity. It is made available under aCC-BY 4.0 International license.

Figure Captions

Figure 1: EEG alpha and slow phase-amplitude coupling during human propofol anesthesia.

(A) Frontal EEG recorded at different propofol doses in human patients (data from (Purdon et al. 2013)). (B) EEG data from A but filtered at alpha (red) and slow (green) frequencies. (C) Stepwise changes in propofol dose throughout the experiment. (D) Comodulogram of alpha frequency amplitude coupling to slow frequency phase of EEG activity in A. (D) Spectrogram of EEG activity in A. Red vertical line marks the time of loss of consciousness.

Figure 2: The simulated thalamocortical network is capable of relay-mode firing.

(A) Illustration of thalamocortical Hodgkin-Huxley network model used for all simulations; for details, see Methods. (B) Rastergrams of each cell/compartment in a relay-mode state, in which each black line represents a spike by each cell/compartment.

Figure 3: Applying direct propofol effects to the thalamocortical network do not enable propofol alpha or slow oscillations.

(A) Rastergrams of each cell/compartment spikes in simulation with direct propofol effects applied. Note the lack of slow or alpha oscillation by excitatory cells throughout the simulation, and that the TC cell population is quiescent. This represents only spiking information, not voltage activity. (B) Voltage trace of a single TC cell. (C) Steady-state curves across voltage for both the “m” activation gate and “h” inactivation gate of the TC cell T-current, with shaded region indicating activation region of “h” gate.

Figure 4: Simulating both direct and indirect propofol effects enables the thalamocortical network to exhibit both slow and alpha oscillations.

bioRxiv preprint doi: https://doi.org/10.1101/2022.02.17.480766; this version posted February 20, 2022. The copyright holder for this preprint (which was not certified by peer review) is the author/funder, who has granted bioRxiv a license to display the preprint in perpetuity. It is made available under aCC-BY 4.0 International license.

Rastergram of a simulation including both direct and indirect propofol effects. Each black line represents a spike by each cell/compartment. Blue highlight indicates time periods of the first distinct dynamic state of the network, and orange highlight indicates the second dynamic state of the network.

Figure 5: Different slow cycles of a low-dose propofol simulation display either trough-max or peak-max alpha-slow PAC.

(A) Representative voltage traces of each cell/compartment during a time period of the simulation expressing trough-max. (B) Representative voltage traces of each cell/compartment type across the low-dose propofol simulation, with time periods of either coupling regime highlighted; blue is trough-max, and orange is peak-max. This is the same simulation as that of Figure 4. (C) Representative voltage traces of each cell/compartment during a time period of the simulation expressing peak-max. (D) Rastergram of all spiking activity during the indicated trough-max time range of the simulation. (E) Rastergram of all spiking activity across the simulation, with coupling regimes highlighted. (F) Rastergram of all spiking activity during the indicated peak-max time range of the simulation.

Figure 6: During a peak-max time period, both sets of synaptic currents are high only near cortical UP states.

(A) Example voltage traces of each cell/compartment type across the low-dose propofol simulation. The red box indicates which peak-max time window is explored in the rest of the figure. (B) Example voltage trace of receiving PYdr compartment of a TC→PY synapse. (C) Example voltage trace of a source TC cell of a TC→PY synapse. (D) Total TC→PY synaptic AMPA currents. (E) Example voltage trace of receiving PYdr compartment of a PY→PY synapse. (F) Example voltage trace of a source PYso compartment of a PY→PY synapse. (G) Total PY→PY synaptic AMPA currents.

bioRxiv preprint doi: https://doi.org/10.1101/2022.02.17.480766; this version posted February 20, 2022. The copyright holder for this preprint (which was not certified by peer review) is the author/funder, who has granted bioRxiv a license to display the preprint in perpetuity. It is made available under aCC-BY 4.0 International license.

Figure 7: During peak-max time periods in a low-dose propofol simulation, both TC→PY and PY→PY synaptic currents are high during the alpha bursting and cortical UP states, enabling cooperation in the final signal.

(A) TC→PY synaptic current during the peak-max time period from Figure 6. (B) PY→PY synaptic current during the peak-max time period from Figure 6. (C) Combination of TC→PY and PY→PY synaptic currents. (D) slow-phase alpha-amplitude comodulogram of combined synaptic currents for the entire simulation.

Figure 8: During trough-max, TC→PY synapses produce more current in the trough, while weaker PY→PY synapses produced peak-max currents.

(A) Example voltage traces of each cell/compartment type across the low-dose propofol simulation. The red box indicates which trough-max time period is explored in the rest of the figure. (B) Example voltage trace of a receiving PYdr compartment of a TC→PY synapse. (C) Example voltage trace of a source TC cell of a TC→PY synapse. (D) Total TC→PY synaptic AMPA currents. (E) Zoom of D, showing the slow-phase modulation of the alpha oscillation amplitude across TC→PY synapses. Dashed lines indicate where this synaptic current is maximal. (F) Example voltage trace of a receiving PYdr compartment of a PY→PY synapse. (G) Example voltage trace of a source PYso compartment of a PY→PY synapse. (H) Total PY→PY synaptic AMPA currents. Note the large difference in amplitude between TC→PY and PY→PY synapses.

Figure 9: During trough-max, TC→PY synaptic currents dominate PY→PY synaptic currents.

(A) TC→PY synaptic current during trough-max time period from Figure 8. (B) PY→PY synaptic current during trough-max time period from Figure 8. Note the much smaller amplitude than A. (C) Combination of TC→PY and PY→PY synaptic currents, which is almost the same as A. (D) slow-phase

bioRxiv preprint doi: https://doi.org/10.1101/2022.02.17.480766; this version posted February 20, 2022. The copyright holder for this preprint (which was not certified by peer review) is the author/funder, who has granted bioRxiv a license to display the preprint in perpetuity. It is made available under aCC-BY 4.0 International license.

alpha-amplitude comodulogram of combined synaptic currents for the entire simulation, with corresponding trough-max time period indicated.

Figure 10: Cortical pyramidal slow oscillation synchronization is associated with the degree of network trough-max PAC versus peak-max conditions.

Trough-max: (A) Example trace of total TC→PYdr AMPA current, showing alpha-slow trough-max. (B) Rastergram of PYdr compartment spikes and TC cell spikes, where each black pixel represents a spike. Note the weakly synchronous slow component in the cortex and persistent propofol alpha in the thalamus. PYdr and PYso activity for any one cell is virtually identical. (C) Example trace of total corticothalamic PYso→TC AMPA current, showing UP-grouped firing. Peak-max PAC: (D) Example trace of total TC→PYdr AMPA current, showing alpha-slow peak-max. (E) Rastergram of PYdr compartment spikes and TC cell spikes. Note the strong synchronicity of UP/DOWN states and thalamic alpha oscillations only near PYdr UP states. (F) Example trace of total corticothalamic PYso→TC AMPA current, showing slow-synchronous corticothalamic activity that is grouped more strongly.

Figure 11: Increasing indirect effects of propofol shifts the low-dose, trough-max preferring network to a high-dose, peak-max preferring one.

Graphic illustrating different inputs and output results of each simulation class. All simulations show different trough-max and peak-max during different slow cycles, but the proportion of trough-max versus peak-max is variable across simulations.

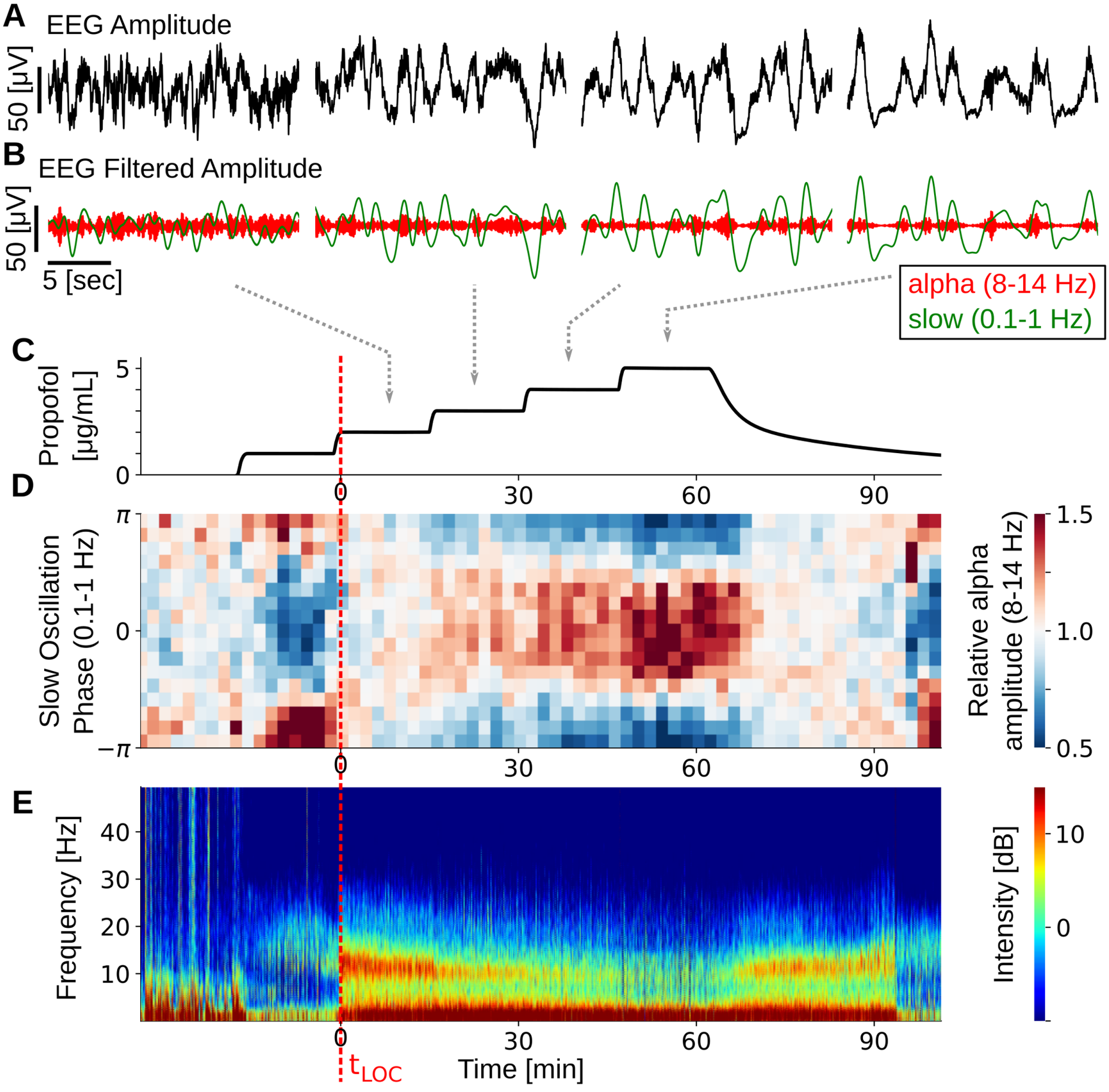
A
EEG Amplitude
50 [μV]
B
EEG Filtered Amplitude
50 [μV]
5 [sec]
alpha (8-14 Hz)
slow (0.1-1 Hz)
C
Propofol [μg/mL]
5
0
0
30
60
90
D
Slow Oscillation Phase (0.1-1 Hz)
π
0
−π
0
30
60
90
Relative alpha amplitude (8-14 Hz)
1.5
1.0
0.5
E
Frequency [Hz]
40
30
20
10
0
30
60
90
Time [min]
t_{LOC}
Intensity [dB]
10
0

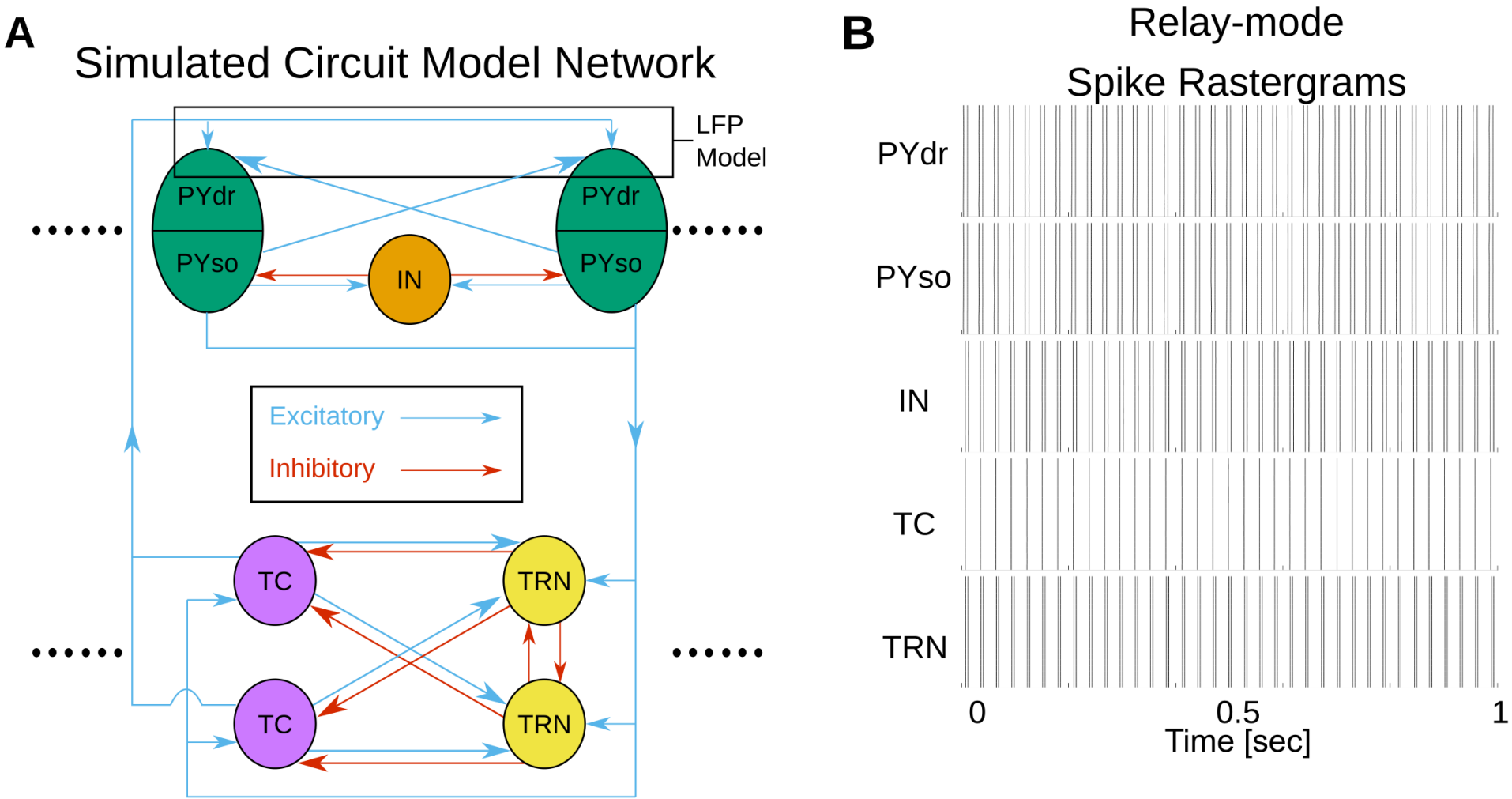
A
Simulated Circuit Model Network
LFP
Model
PYdr
PYso
IN
PYdr
PYso
Excitatory
Inhibitory
TC
TRN
TC
TRN
B
Relay-mode
Spike Rastergrams
PYdr
PYso
IN
TC
TRN
0
0.5
1
Time [sec]

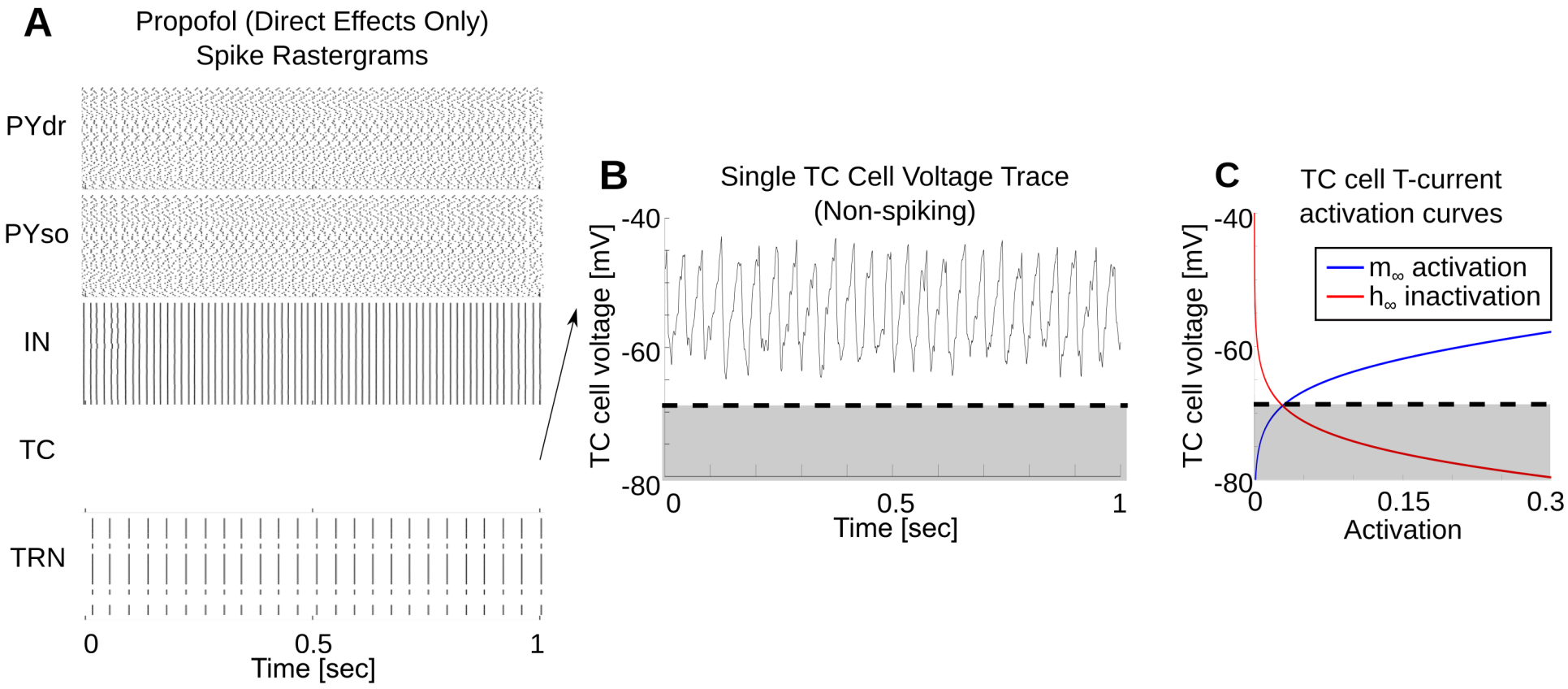
A
Propofol (Direct Effects Only)
Spike Rastergrams
PYdr
PYso
IN
TC
TRN
0
0.5
1
Time [sec]
B
Single TC Cell Voltage Trace
(Non-spiking)
TC cell voltage [mV]
-40
-60
-80
0
0.5
1
Time [sec]
C
TC cell T-current
activation curves
TC cell voltage [mV]
-40
-60
-80
m∞ activation
h∞ inactivation
0
0.15
0.3
Activation

Simulation Spike Rastergram (Direct and Indirect Propofol Effects)

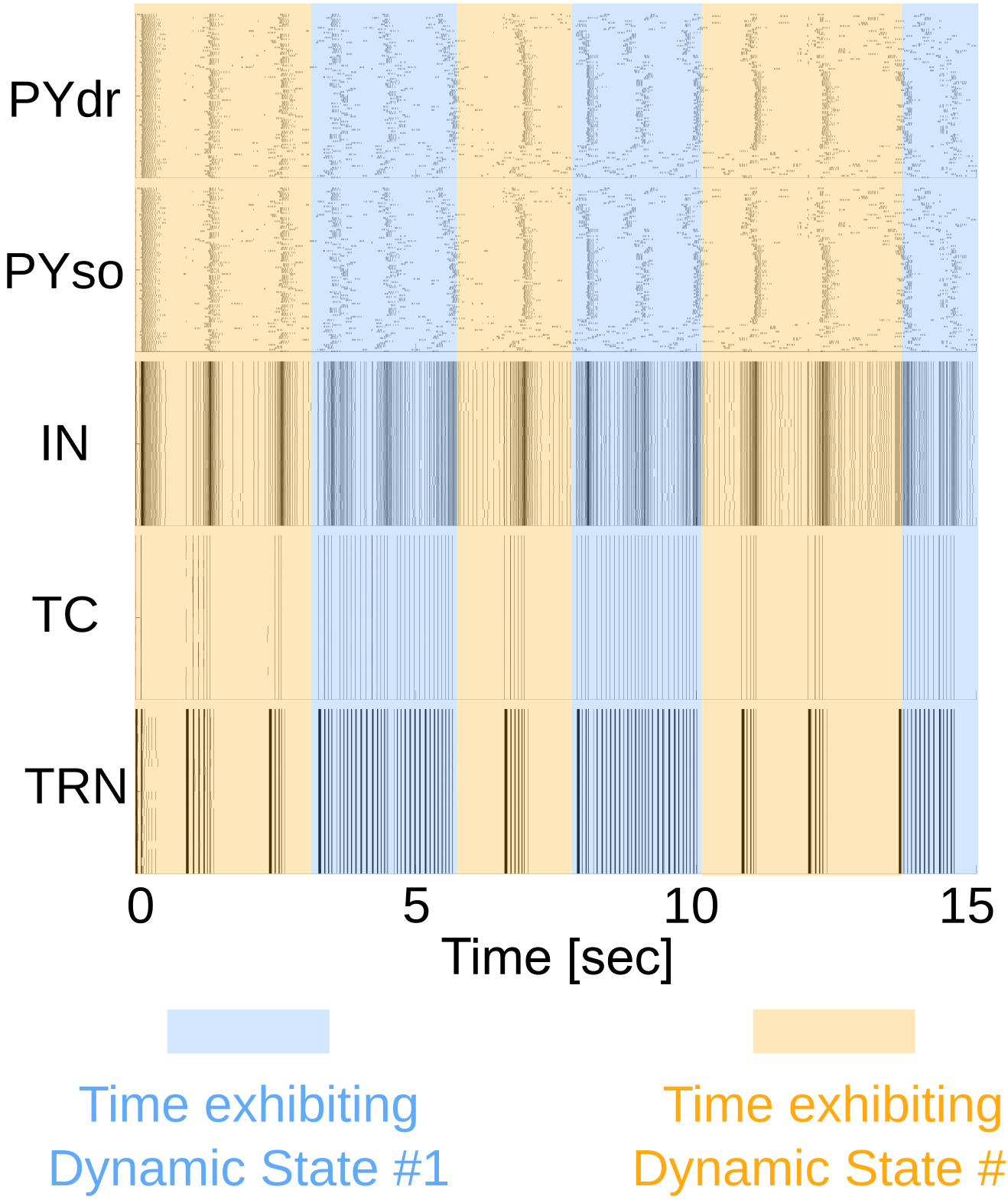

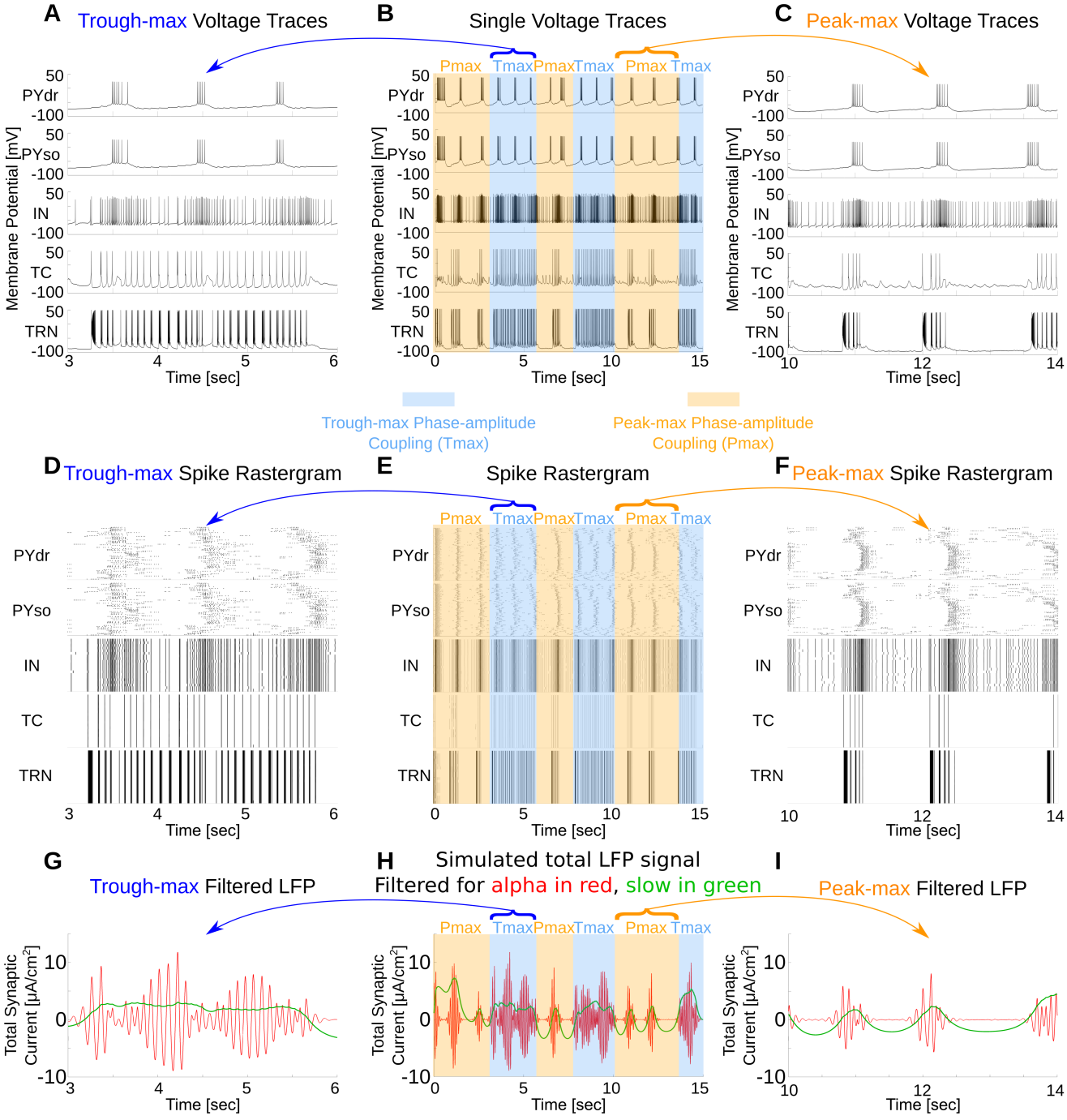
A
Trough-max Voltage Traces
B
Single Voltage Traces
C
Peak-max Voltage Traces
Pmax
Tmax
Pmax
Tmax
Pmax
Tmax
PYdr
PYso
IN
TC
TRN
Membrane Potential [mV]
50
-100
Time [sec]
Trough-max Phase-amplitude Coupling (Tmax)
Peak-max Phase-amplitude Coupling (Pmax)
D
Trough-max Spike Rastergram
E
Spike Rastergram
F
Peak-max Spike Rastergram
G
Trough-max Filtered LFP
H
Simulated total LFP signal
Filtered for alpha in red, slow in green
I
Peak-max Filtered LFP
Total Synaptic Current [μA/cm²]
10
0
-10

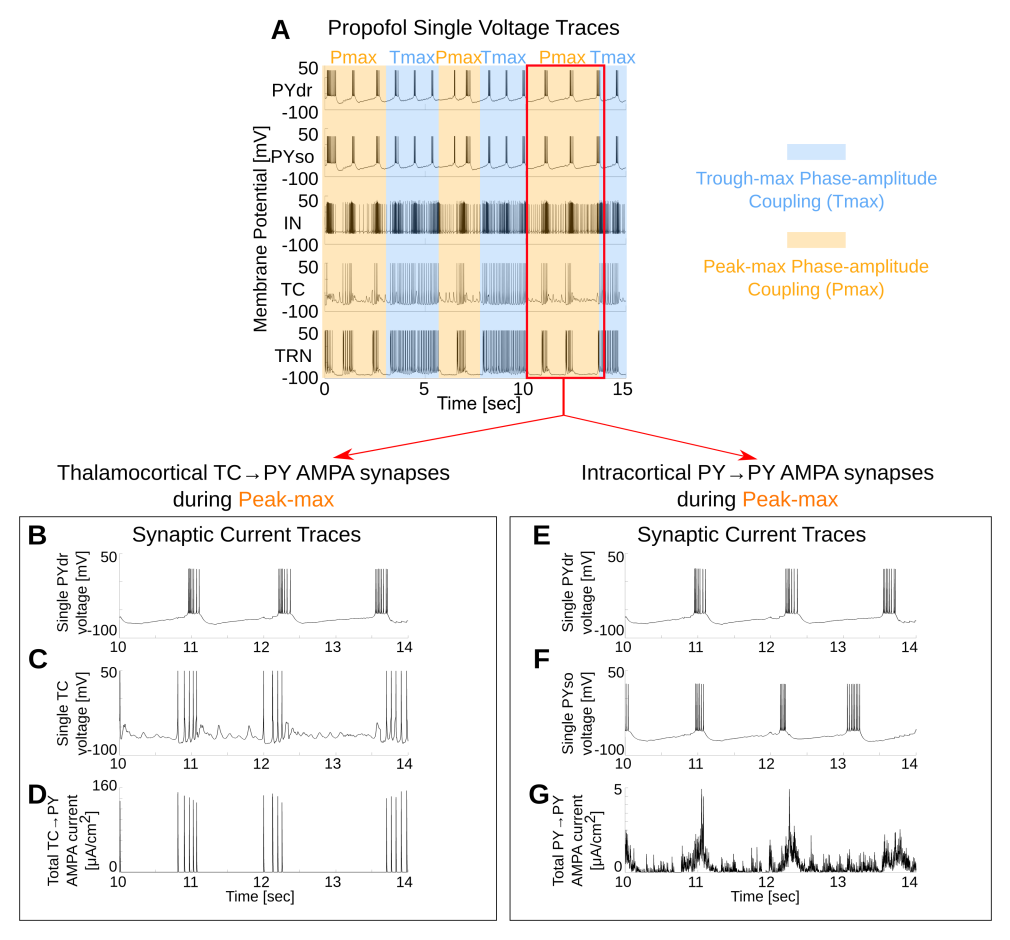
A
Propofol Single Voltage Traces
Pmax
Tmax
Pmax
Tmax
Pmax
Tmax
PYdr
PYso
IN
TC
TRN
50
-100
Membrane Potential [mV]
0
5
10
15
Time [sec]
Trough-max Phase-amplitude Coupling (Tmax)
Peak-max Phase-amplitude Coupling (Pmax)
Thalamocortical TC→PY AMPA synapses during Peak-max
Intracortical PY→PY AMPA synapses during Peak-max
B
Synaptic Current Traces
Single PYdr voltage [mV]
C
Single TC voltage [mV]
D
Total TC→PY AMPA current [μA/cm2]
160
0
Time [sec]
E
Synaptic Current Traces
Single PYdr voltage [mV]
F
Single PYso voltage [mV]
G
Total PY→PY AMPA current [μA/cm2]
5
Time [sec]

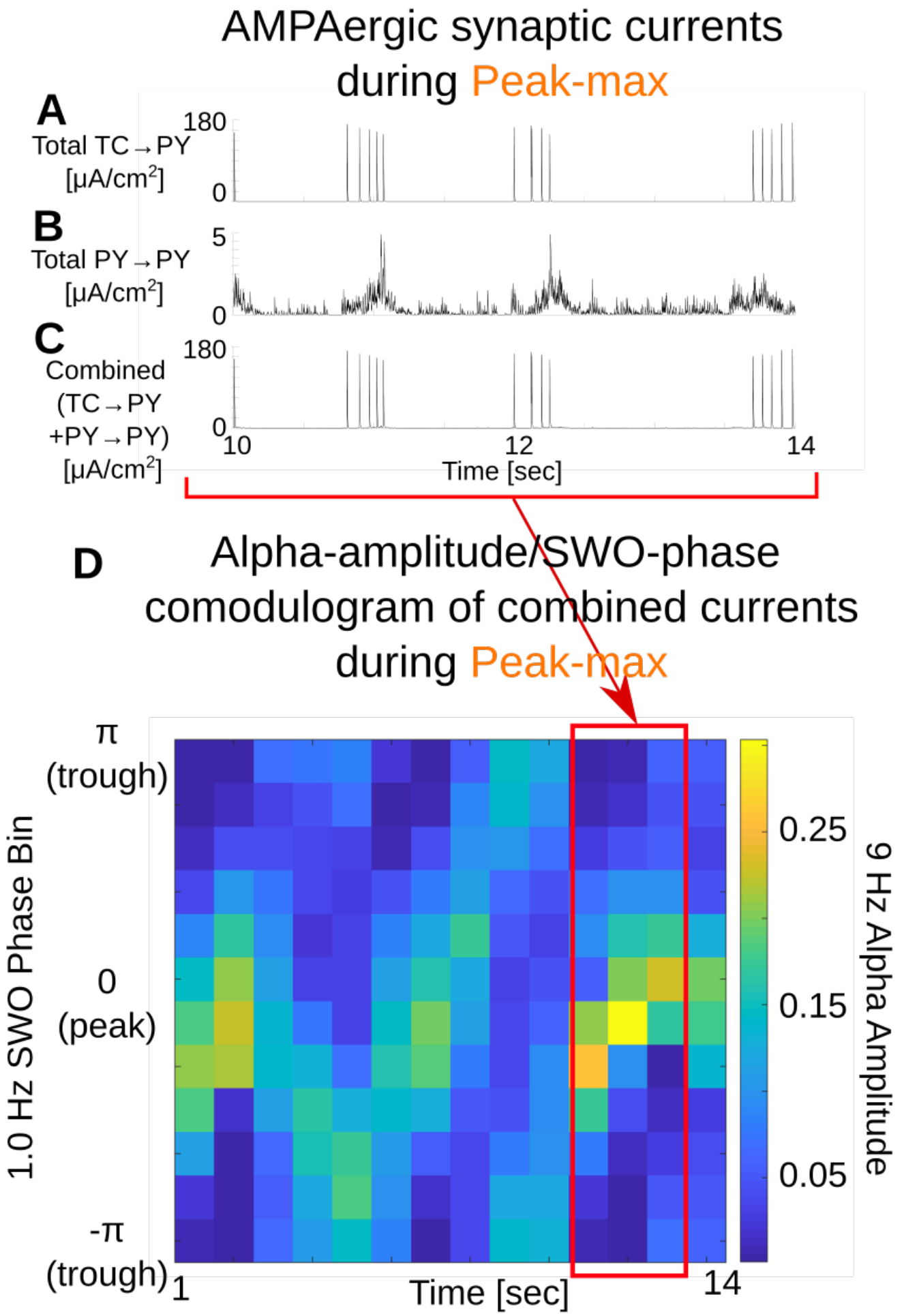
AMPAergic synaptic currents during Peak-max
A
Total TC → PY [μA/cm²]
180
0
B
Total PY → PY [μA/cm²]
5
0
C
Combined (TC → PY +PY → PY) [μA/cm²]
180
0
10
12
14
Time [sec]
D
Alpha-amplitude/SWO-phase comodulogram of combined currents during Peak-max
π (trough)
0 (peak)
-π (trough)
1.0 Hz SWO Phase Bin
1
14
Time [sec]
0.25
0.15
0.05
9 Hz Alpha Amplitude

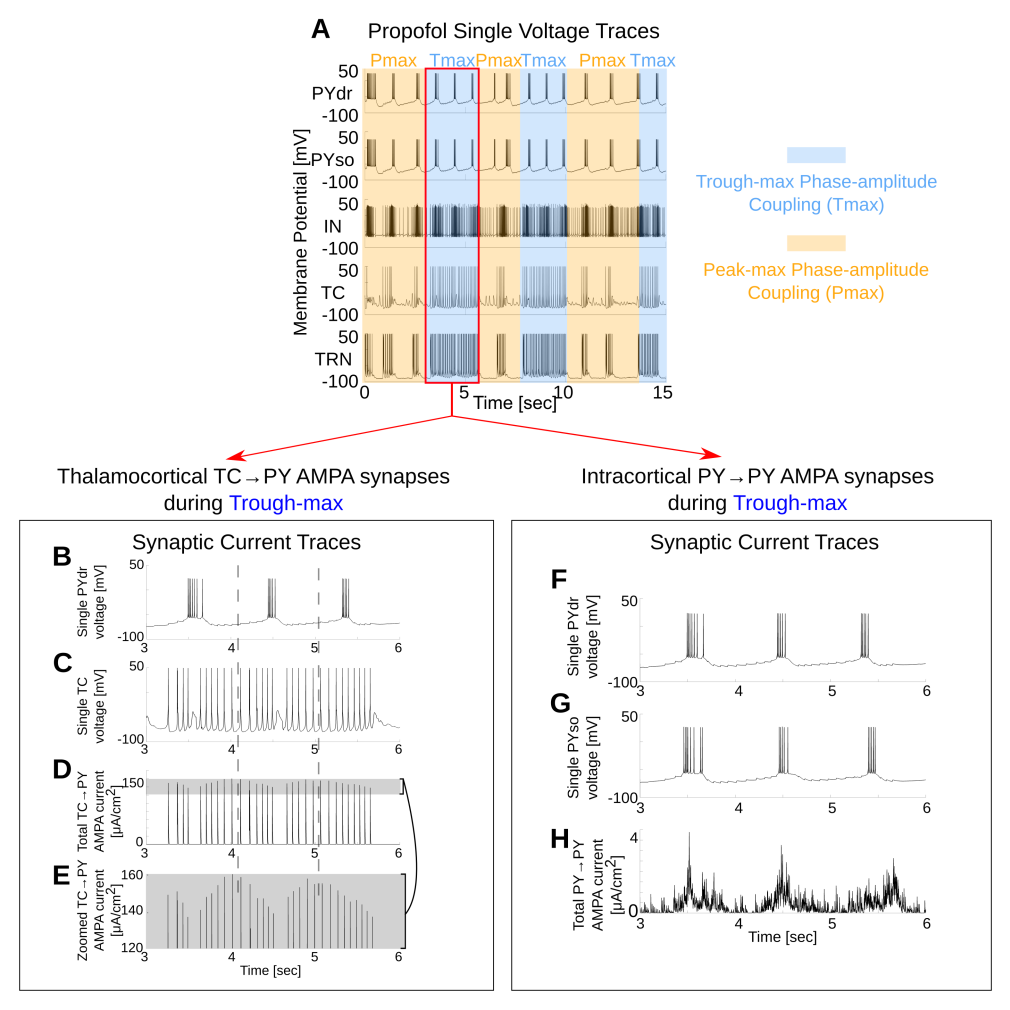
A
Propofol Single Voltage Traces
Pmax
Tmax
Pmax
Tmax
Pmax
Tmax
PYdr
PYso
IN
TC
TRN
Membrane Potential [mV]
Time [sec]
Trough-max Phase-amplitude Coupling (Tmax)
Peak-max Phase-amplitude Coupling (Pmax)
Thalamocortical TC→PY AMPA synapses during Trough-max
Intracortical PY→PY AMPA synapses during Trough-max
Synaptic Current Traces
B
Single PYdr voltage [mV]
C
Single TC voltage [mV]
D
Total TC→PY AMPA current [μA/cm2]
E
Zoomed TC→PY AMPA current [μA/cm2]
Time [sec]
Synaptic Current Traces
F
Single PYdr voltage [mV]
G
Single PYso voltage [mV]
H
Total PY→PY AMPA current [μA/cm2]
Time [sec]

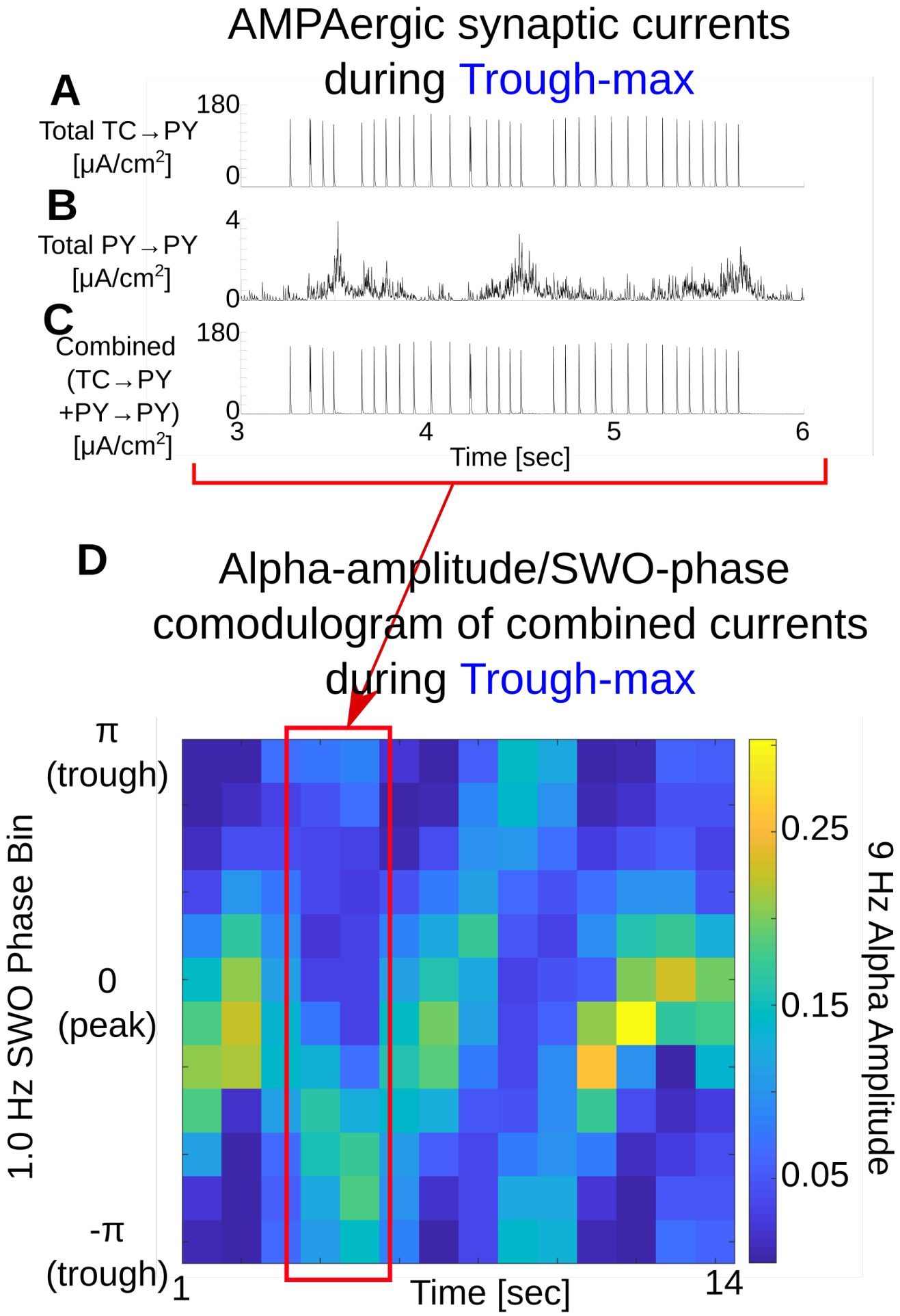
AMPAergic synaptic currents during Trough-max
A
Total TC → PY [μA/cm²]
180
0
B
Total PY → PY [μA/cm²]
4
0
C
Combined (TC → PY +PY → PY) [μA/cm²]
180
0
3
4
5
6
Time [sec]
D
Alpha-amplitude/SWO-phase comodulogram of combined currents during Trough-max
π (trough)
0 (peak)
-π (trough)
1.0 Hz SWO Phase Bin
1
14
Time [sec]
0.25
0.15
0.05
9 Hz Alpha Amplitude

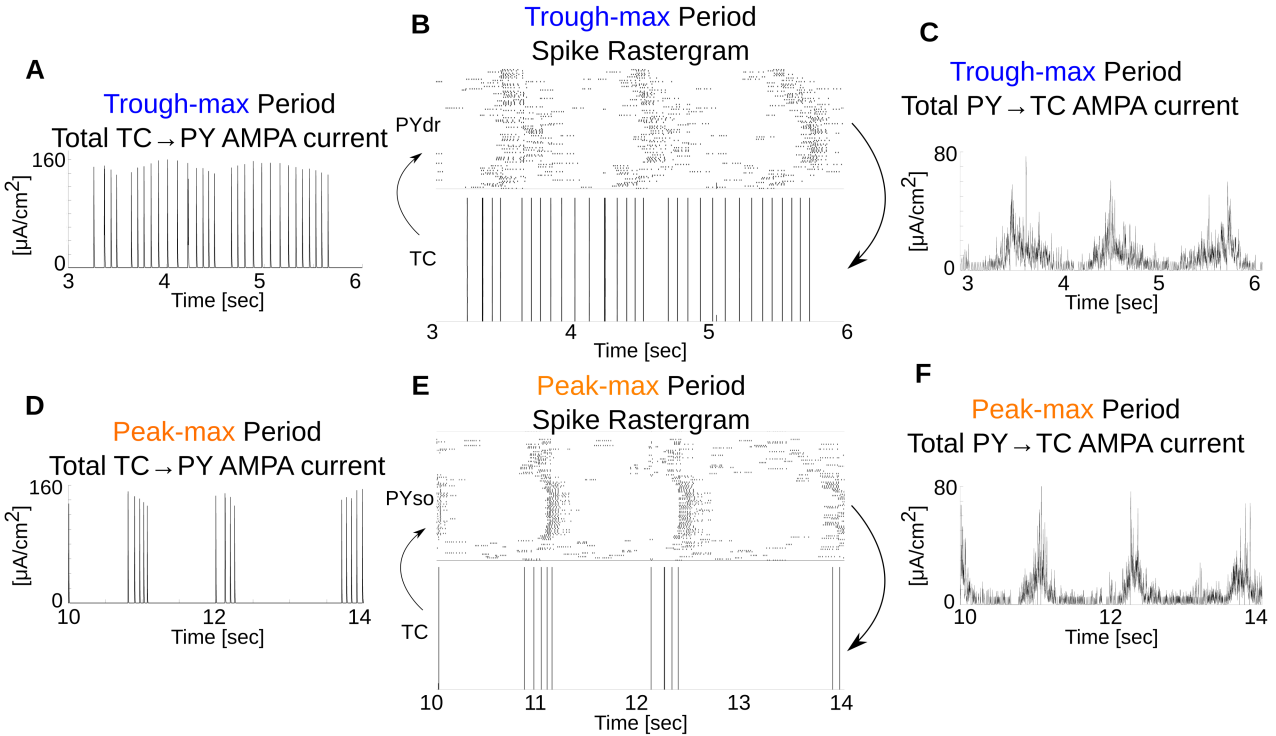
A
Trough-max Period
Total TC → PY AMPA current
160
0
[μA/cm2]
3
4
5
6
Time [sec]
B
Trough-max Period
Spike Rastergram
PYdr
TC
3
4
5
6
Time [sec]
C
Trough-max Period
Total PY → TC AMPA current
80
0
[μA/cm2]
3
4
5
6
Time [sec]
D
Peak-max Period
Total TC → PY AMPA current
160
0
[μA/cm2]
10
12
14
Time [sec]
E
Peak-max Period
Spike Rastergram
PYso
TC
10
11
12
13
14
Time [sec]
F
Peak-max Period
Total PY → TC AMPA current
80
0
[μA/cm2]
10
12
14
Time [sec]
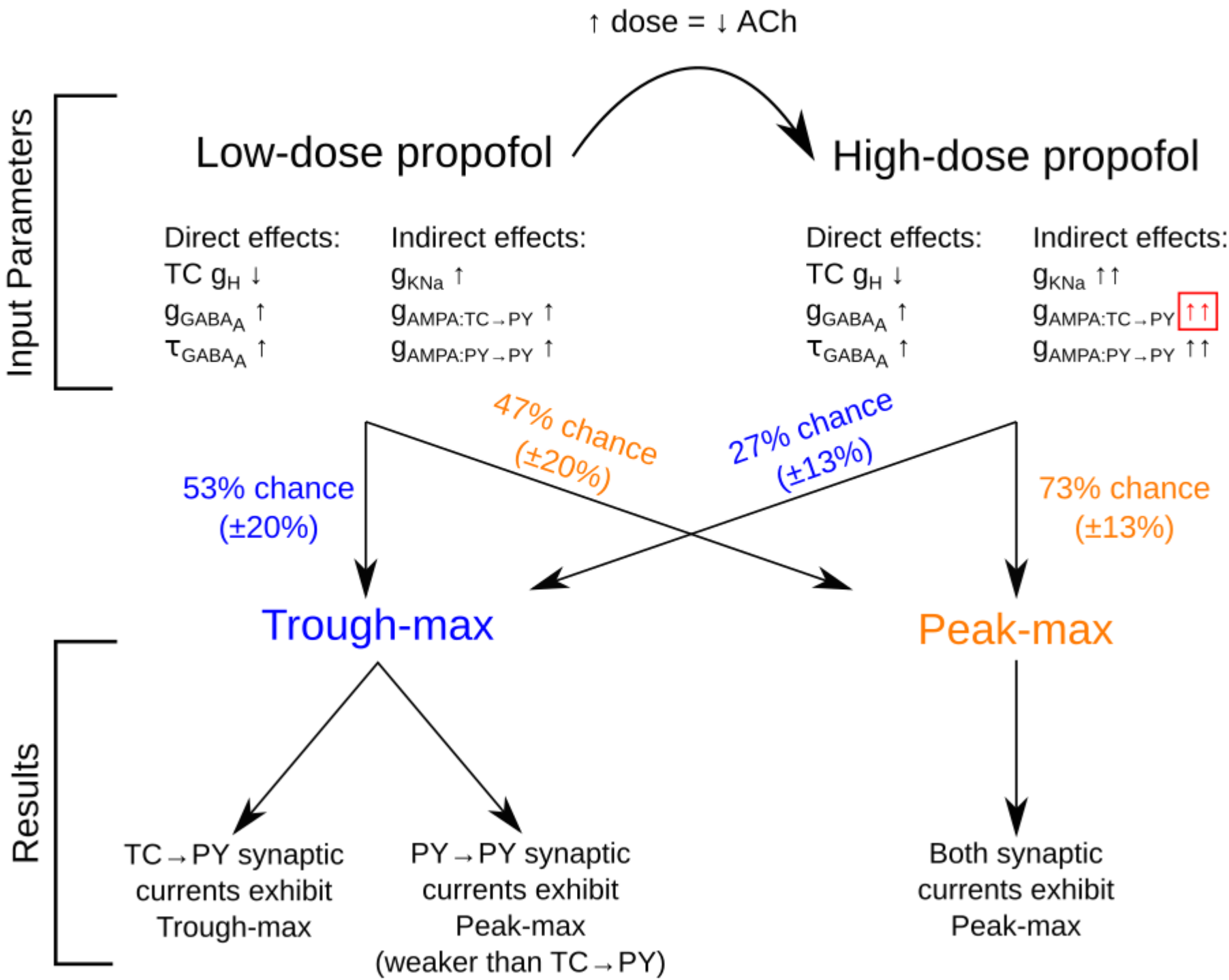
Breakdown of dose-specific simulation results